Article

Cell Reports

The mTOR and PP2A Pathways Regulate PHD2 Phosphorylation to Fine-Tune HIF1α Levels and Colorectal Cancer Cell Survival under Hypoxia

Graphical Abstract

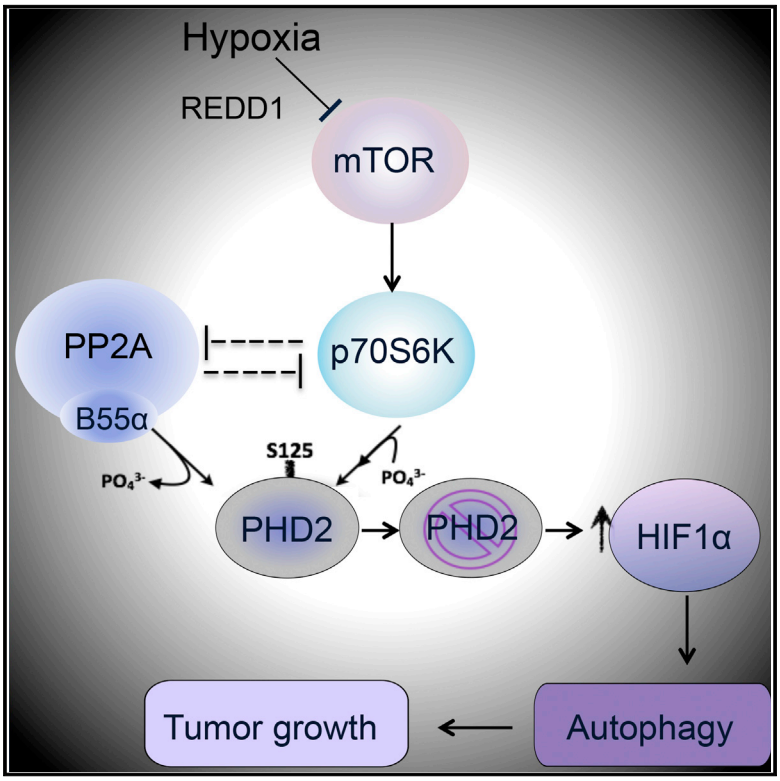

Authors

Giusy Di Conza, Sarah Trusso Cafarello, Stefan Loroch, ..., Thomas Kietzmann, Fabiola Moretti, Massimiliano Mazzone

Correspondence

massimiliano.mazzone@vib-kuleuven.be

In Brief

Di Conza et al. find that PP2A/B55α dephosphorylates and partly inactivates PHD2, leading to augmented HIF1α and CRC cell survival in hypoxia through autophagy. Dephosphorylated PHD2 and B55α accumulate in CRC human specimens versus normal colon, and B55α targeting impairs CRC neoplastic growth in vitro and in mice.

Highlights

- PHD2 is phosphorylated at Ser125 by P70S6K and dephosphorylated by PP2A/B55α
- PHD2 dephosphorylation impairs its function, resulting in increased HIF1α accumulation
- HIF1α promotes CRC survival in hypoxia via autophagy in a PHD2/B55α-dependent fashion
- B55α silencing blocks CRC tumor growth in vitro and in vivo; this is PHD2 dependent

Di Conza et al., 2017, Cell Reports *18*, 1699–1712
February 14, 2017
http://dx.doi.org/10.1016/j.celrep.2017.01.051

Cell Reports
Article

The mTOR and PP2A Pathways Regulate PHD2 Phosphorylation to Fine-Tune HIF1α Levels and Colorectal Cancer Cell Survival under Hypoxia

Giusy Di Conza,[1,2] Sarah Trusso Cafarello,[1,2] Stefan Loroch,[3] Daniela Mennerich,[4] Sofie Deschoemaeker,[1,2] Mario Di Matteo,[1,2] Manuel Ehling,[1,2] Kris Gevaert,[5,6] Hans Prenen,[7] Rene Peiman Zahedi,[3] Albert Sickmann,[3,8,9] Thomas Kietzmann,[4] Fabiola Moretti,[10] and Massimiliano Mazzone[1,2,11,*]

[1]Laboratory of Tumor Inflammation and Angiogenesis, Center for Cancer Biology, VIB, 3000 Leuven, Belgium
[2]Laboratory of Tumor Inflammation and Angiogenesis, Department of Oncology, Center for Cancer Biology, KU Leuven, 3000 Leuven, Belgium
[3]Leibniz Institut für Analytische Wissenschaften - ISAS - e.V., 44227 Dortmund, Germany
[4]Faculty of Biochemistry and Molecular Medicine and Biocenter Oulu, University of Oulu, 90220 Oulu, Finland
[5]Department of Medical Protein Research, VIB, 9000 Ghent, Belgium
[6]Department of Biochemistry, Ghent University, 9000 Ghent, Belgium
[7]Digestive Oncology Unit, Department of Oncology, University Hospital Gasthuisberg, KU Leuven, 3000 Leuven, Belgium
[8]Department of Chemistry, College of Physical Sciences, University of Aberdeen, Aberdeen AB24 3UE, Scotland, UK
[9]Medizinisches Proteom Center, Ruhr Universität Bochum, 44801 Bochum, Germany
[10]Institute of Cell Biology and Neurobiology, National Research Council of Italy, 00143 Roma, Italy
[11]Lead Contact
*Correspondence: massimiliano.mazzone@vib-kuleuven.be
http://dx.doi.org/10.1016/j.celrep.2017.01.051

SUMMARY

Oxygen-dependent HIF1α hydroxylation and degradation are strictly controlled by PHD2. In hypoxia, HIF1α partly escapes degradation because of low oxygen availability. Here, we show that PHD2 is phosphorylated on serine 125 (S125) by the mechanistic target of rapamycin (mTOR) downstream kinase P70S6K and that this phosphorylation increases its ability to degrade HIF1α. mTOR blockade in hypoxia by REDD1 restrains P70S6K and unleashes PP2A phosphatase activity. Through its regulatory subunit B55α, PP2A directly dephosphorylates PHD2 on S125, resulting in a further reduction of PHD2 activity that ultimately boosts HIF1α accumulation. These events promote autophagy-mediated cell survival in colorectal cancer (CRC) cells. B55α knockdown blocks neoplastic growth of CRC cells in vitro and in vivo in a PHD2-dependent manner. In patients, CRC tissue expresses higher levels of REDD1, B55α, and HIF1α but has lower phospho-S125 PHD2 compared with a healthy colon. Our data disclose a mechanism of PHD2 regulation that involves the mTOR and PP2A pathways and controls tumor growth.

INTRODUCTION

Tumor hypoxia correlates with unfavorable disease outcome, malignancy, and resistance to therapy (De Bock et al., 2011). The main executors of the cellular response to hypoxia are the hypoxia-inducible factors (HIFs) HIF1 and HIF2, which are negatively regulated by the HIF prolyl hydroxylase (PHD) family members PHD1, PHD2, and PHD3. Following hydroxylation in specific prolyl residues, the alpha subunits of HIF1 and HIF2 are targeted for ubiquitination and proteasomal degradation (Epstein et al., 2001; Keith et al., 2011).

Although the activity of PHDs is reduced by hypoxia, this is a graded effect, and, because of their high affinity for oxygen (K_M = 100–250 μM), significant PHD activity is still observed at 1% oxygen (Chan et al., 2005; Epstein et al., 2001; Pan et al., 2007; Stolze et al., 2004). Indeed, several reports document that HIFs still become hydroxylated under nearly anoxic conditions (Chan et al., 2005; Epstein et al., 2001). Under these conditions, manipulation of PHD levels or activity can be a key determinant in the hydroxylation rate of HIFα (Chan et al., 2005; Epstein et al., 2001; Pan et al., 2007; Stolze et al., 2004). Transcriptional induction of PHD2 and PHD3 (*EGLN1* and *EGLN3*, respectively) during chronic hypoxia presumably prevents a deleterious HIF response upon reoxygenation (Appelhoff et al., 2004; Epstein et al., 2001; Ginouvès et al., 2008).

Although HIF levels have mostly been associated with a poor prognosis of several tumor histotypes, the correlation between PHD abundance and cancer progression is less clear (Jokilehto and Jaakkola, 2010). This is likely due to the fact that mechanisms besides protein level regulation, including oxygen, cofactor bioavailability, and post-translational modifications (e.g., SUMOylation), can regulate the enzymatic function of PHDs (Jokilehto and Jaakkola, 2010; Núñez-O'Mara et al., 2015; Ortmann et al., 2016). The presence of phosphorylation sites in PHD2 has been predicted (http://www.phosphonet.ca), but their functional role is unclear.

mTOR is one of the main kinases involved in the regulation of protein synthesis and cell growth in response to nutrients and

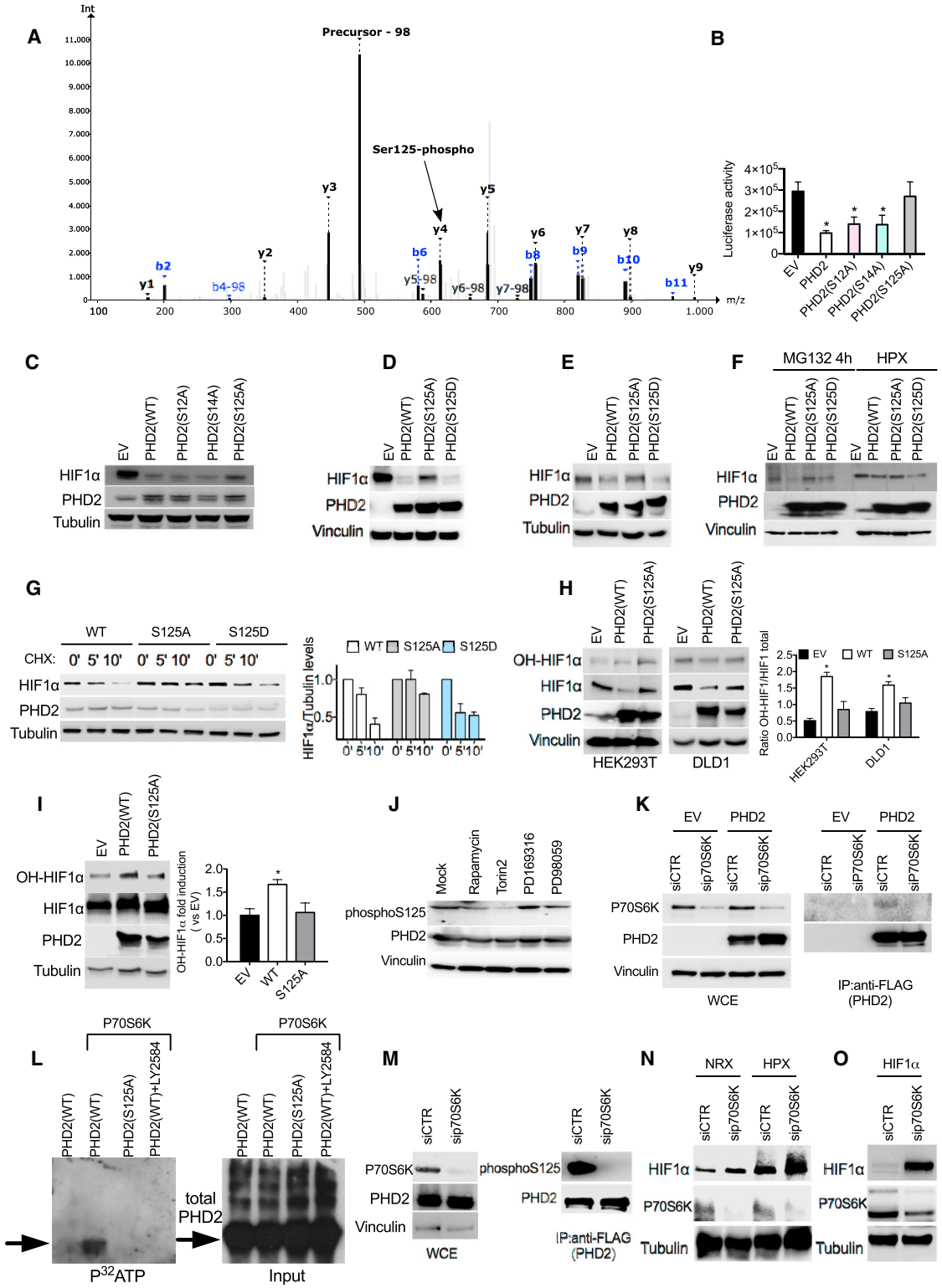

Figure 1. Phosphorylation of S125 by P70S6K Is Important to Control HIF1α Levels

(A) MS/MS spectrum of NH_2-AKPPADPAAAAS$^{<P>}$PCR-COOH (S$^{<P>}$ indicates phosphoserine). Nine of 15 amino acids, including the phosphorylated serine, are covered by a ladder of y-type fragment ions. The neutral loss peak (−98 Da) characteristic for phosphorylated peptides is the most intense peak of the spectrum at 492.9 mass-to-charge ratio (m/z).

(legend continued on next page)

growth factors. When normal or cancer cells are exposed to starvation, mTOR is inhibited, and autophagy is induced mainly as a survival response. mTOR is also involved in the hypoxia response. In particular, HIF1α stabilization leads to early transcription of REDD1, which works as a negative regulator of mTOR and restrains its activity in hypoxia (Brugarolas et al., 2004). Full inactivation of mTOR also requires the engagement of the PP2A phosphatase (Hartley and Cooper, 2002; Peterson et al., 1999; Roberts et al., 2014), further blocking this pathway by directly dephosphorylating and inhibiting P70S6-kinase (P70S6K) downstream of mTOR.

PP2A is a ubiquitously expressed serine-threonine phosphatase. It is a trimeric complex formed by a catalytic C subunit, a scaffold A subunit, and a regulatory B subunit, which confers specificity of PP2A for selective substrates. Fifteen B subunit genes encoding 26 different isoforms give rise to more than 100 combinations of the PP2A holoenzyme, leading to a large spectrum of biological activities (Seshacharyulu et al., 2013). In cancer, PP2A is considered to be a tumor suppressor because its main inhibitor, okadaic acid, was shown to have tumor-promoting activity (Bialojan and Takai, 1988). However, the complexity of the PP2A structure suggests that the presence of different B subunits might determine different phenotypes in the context of cancer.

RESULTS

P70S6K-Mediated Phosphorylation of PHD2 on S125 Controls HIF1α Levels

Mass spectrometry analysis of wild-type PHD2 ($PHD2^{WT}$) revealed three phosphorylation sites in S12, S14, and S125. Mutation of S125 to alanine ($PHD2^{S125A}$) impaired PHD2 ability to reduce the signal emitted by a luciferase fused to an oxygen-dependent degradation domain (Luc-ODDD) or to degrade HIF1α compared with wild-type PHD2 (Figures 1A–1C; Table S1), suggesting that phosphorylation at S125 modulates its function. In contrast, $PHD2^{S12A}$ or $PHD2^{S14A}$ mutants displayed similar activity as $PHD2^{WT}$ (Figures 1B and 1C). To further investigate the effect of PHD2 mutants on HIF1α levels, we transfected HEK293T or DLD1 cells with $PHD2^{WT}$, $PHD2^{S125A}$, or $PHD2^{S125D}$ (which mimics constitutive phosphorylation). $PHD2^{WT}$ as well as $PHD2^{S125D}$ induced degradation of both exogenous and endogenous HIF1α (Figures 1D and 1E; Table S1), whereas the mutant $PHD2^{S125A}$ showed impaired function. Similarly, HT29 cells exposed to the proteasome inhibitor MG132 showed partial HIF1α degradation upon overexpression of $PHD2^{WT}$ and $PHD2^{S125D}$ but not of $PHD2^{S125A}$ (Figure 1F; Table S1). Prolonged exposure to MG132 overruled the differential activity of all PHD2 isoforms ($PHD2^{WT}$, $PHD2^{S125A}$, and $PHD2^{S125D}$), as indicated by the equalized HIF1α levels (Figure S1A). In hypoxia, the activity of these PHD2 isoforms on HIF1α resembled what was observed previously (Figure 1F; Table S1). Moreover, the half-life of HIF1α was strongly reduced in the presence of $PHD2^{WT}$ and $PHD2^{S125D}$, whereas, under the same conditions, expression of $PHD2^{S125A}$ correlated with a longer HIF1α half-life (Figure 1G). To test whether PHD2 phosphorylation might affect its enzymatic activity, we measured HIF1α hydroxylation. In both HEK293T and DLD1 cells, hydroxylation of overexpressed HIF1α was 40% to 55% lower in the presence of $PHD2^{S125A}$ than with $PHD2^{WT}$ (Figure 1H). Similarly, upon treatment with the proteasome inhibitor MG132 (which equalizes the total levels of HIF1α under all conditions), hydroxylation of endogenous HIF1α by $PHD2^{S125A}$ was halved compared with the amount detected in the presence of $PHD2^{WT}$ (Figure 1I). These data indicate that the lack of phosphorylation of PHD2 on S125 impairs its hydroxylase function, leading to a longer HIF1α half-life.

To unveil the kinase responsible for PHD2 phosphorylation, we blocked the predicted PHD serine kinases (http://www.phosphonet.ca) and used a specific phospho-PHD2 antibody

(B) Luciferase activity of HEK293T cells stably overexpressing an oxygen-dependent degradable luciferase (Luc-ODDD) transfected with plasmids carrying wild-type (WT) or mutant PHD2 (S12A, S14A, and S125A) or an empty vector (EV) as a control.
(C) Western blot (WB) of HEK293T cells transfected with HIF1α, alone (EV) or in combination with WT or mutant PHD2 (S12A, S14A, and S125A).
(D) WB of HEK293T cells transfected with HIF1α, alone (EV) or in combination with $PHD2^{WT}$, $PHD2^{S125A}$, or $PHD2^{S125D}$.
(E) WB of DLD1 cells transfected with $PHD2^{WT}$, $PHD2^{S125A}$, and $PHD2^{S125D}$ and exposed to hypoxia for 4 hr.
(F) HT29 cells were transfected with an EV or with $PHD2^{WT}$, $PHD2^{S125A}$, and $PHD2^{S125D}$. After 16 hr, cells were treated with the proteasome inhibitor MG132 or exposed to hypoxic conditions for 4 hr, and whole cell extracts (WCEs) were analyzed by WB.
(G) DLD1 cells were transfected with $PHD2^{WT}$, $PHD2^{S125A}$, and $PHD2^{S125D}$. After 16 hr, cells were treated with cycloheximide for the indicated time, and WCEs were analyzed by WB.
(H) HEK293T or DLD1 cells were transfected with HIF1α, alone (EV) or in combination with $PHD2^{WT}$ or $PHD2^{S125A}$. Hydroxylation of HIF1α was detected by using antibody against OH-HIF1α.
(I) WB of DLD1 cells transfected with $PHD2^{WT}$, $PHD2^{S125A}$, and $PHD2^{S125D}$ and treated with MG132 (10 μM) for 8 hr.
(J) WB of HEK293T cells transfected with PHD2 treated with 1 μM Rapamycin, 200 nM Torin2, 10 μM PD169316, and 10 μM PD19058 for 16 hr.
(K) DLD1 cells were transfected with either EV or FLAG-PHD2 and with a control (siCTR) or a small interfering RNA (siRNA) targeting P70S6K (siP70S6K). After 24 hr, cells were lysed, and WCEs were analyzed by WB (left). 1 mg of EV or FLAG-PHD2 lysate was immunoprecipitated using anti-FLAG M2 beads to detect endogenous P70S6K kinase (right).
(L) Purified FLAG-PHD2 and PHD2 S125 proteins were phosphorylated with active P70S6K kinase in the presence of [^{32}P]-γ-ATP for 20 min at 30°C. The specific P70S6K inhibitor LY2584702 was used to a final concentration of 50 μM. Proteins were separated by 10% SDS-PAGE, and incorporated radioactivity was detected by autoradiography (left). A WB of PHD2 input was used as a loading control (right).
(M) HEK293T were transfected with FLAG-PHD2 and silenced with siP70S6K or siCTR. Then cells were lysed, and WCEs were analyzed by WB. 1 mg of EV or FLAG-PHD2 lysate was immunoprecipitated using anti-FLAG M2 beads to detect endogenous phosphorylated PHD2 (right).
(N) WB of DLD1 cells transfected with siCTR or siP70S6K and exposed to hypoxia for 4 hr.
(O) WB of HEK293T cells overexpressing HIF1α and silenced with siP70S6K or siCTR.
All WBs were repeated three times on independent biological replicates. *$p < 0.05$ versus EV in (B) and versus all other conditions in (H) and (I). Graphs show mean ± SEM. See also Figure S1.

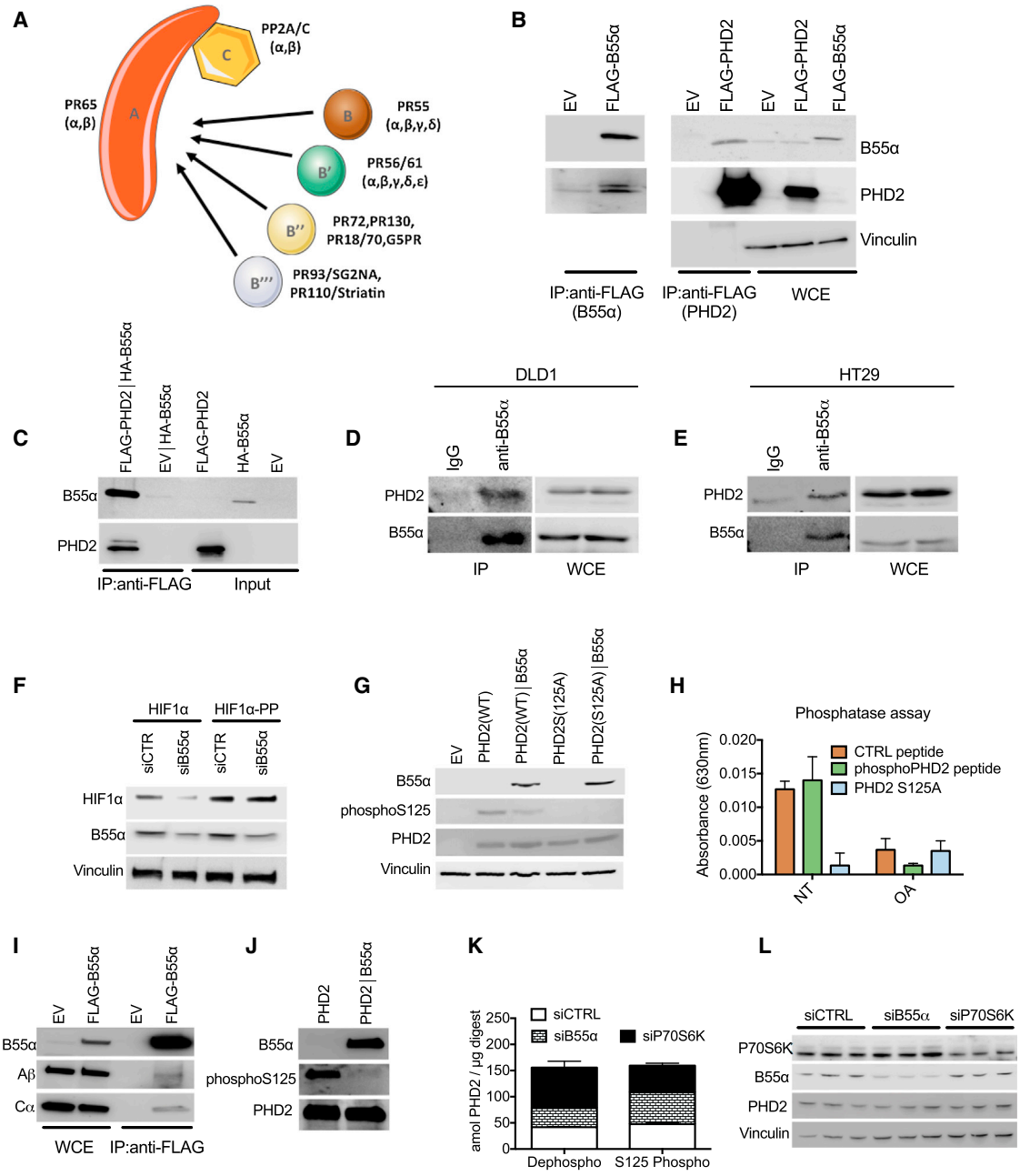

Figure 2. PP2A/B55α Specifically Binds and Dephosphorylates PHD2 in S125

(A) Schematic of the PP2A holoenzyme. Subunits A (scaffold subunit) and C (catalytic subunit) form a complex that can combine with different regulatory B subunits responsible for the substrate and cell type specificity. B55α represents the α isoform of the family PR55.

(B) HEK293T cells were transfected with EV, B55α (FLAG-B55α), or PHD2 (FLAG-PHD2), and WCEs were analyzed by WB (right, WCE). 1 mg of EV or FLAG-B55α lysate was immunoprecipitated using anti-FLAG M2 beads to detect endogenous PHD2. 1 mg of EV or FLAG-PHD2 lysates was immunoprecipitated with anti-FLAG M2 beads to detect endogenous B55α.

(C) In vitro-translated pcDNA3/FLAG-PHD2 (FLAG-PHD2) or pcDNA3/FLAG (EV) was immunoprecipitated with anti-FLAG M2 beads after incubation with in vitro-translated B55α (HA-B55α), and immunocomplexes were detected by WB analysis.

(D and E) WCEs from DLD1 (D) or HT29 (E) were collected and immunoprecipitated with anti-B55α or anti-immunoglobulin G (IgG) as a control, and endogenous PHD2 in immunocomplexes was detected by WB analysis.

(F) WB of DLD1 cells transfected with either HIF1α or an HIF1α proline mutant (HIF1α-PP) and with siCTR or B55α (siB55α).

(G) WB of HEK293T cells transfected with an EV or PHD2 (WT or S125A), alone and in combination with B55α. After 24 hr, WCEs were analyzed by WB.

(H) In vitro phosphatase assay in which two synthetized peptides from PHD2 (WT or mutant sequence) and a positive control peptide were used as substrate of cell-isolated PP2A complex. The result indicates the absorbance released by free phosphate groups following the dephosphorylation reaction. NT, not treated.

(legend continued on next page)

as readout. Torin2 and Rapamycin, both blocking the mTOR pathway, were able to downmodulate phospho-PHD2 (Figure 1J; Table S1). In fact, we found that the serine/threonine kinase P70S6K, an mTOR target, was able to bind (Figure 1K) and directly phosphorylate PHD2 in vitro and in vivo (Figures 1L and 1M). Furthermore, P70S6K knockdown caused increased levels of both hypoxia-induced and overexpressed HIF1α (Figures 1N and 1O). Altogether, these results show that P70S6K phosphorylates PHD2 on S125, leading to enhanced HIF1α degradation.

PP2A/B55α Specifically Binds and Dephosphorylates PHD2 on S125

To assess whether a specific phosphatase complex could interact with PHD2, we performed a stable isotope labeling with amino acids in cell culture (SILAC)-based mass spectrometry analysis from which it emerged that the B55α regulatory subunit of the phosphatase family PP2A was able to co-immunoprecipitate with PHD2 (Table S2; Figure 2A). In HEK293T cells, overexpressed B55α pulls down endogenous PHD2 (Figure 2B, left). Vice versa, overexpressed PHD2 interacts with endogenous B55α (Figure 2B, right). Because in vitro-translated PHD2 and B55α were able to bind each other in a cell-free system (Figure 2C), this binding is direct and does not require other partners. In both DLD1 and HT29 colorectal cancer (CRC) cells, endogenous PHD2 and B55α were able to bind to each other (Figures 2D and 2E; Figure S1B), suggesting that this interaction occurs in different cell lines. PHD2 could pull down the PP2A catalytic subunit Cα as well, but only in the presence of B55α (Figure S1C). This interaction was specific for B55α because PHD2 did not bind in vitro-translated B55β, γ, or δ (Figure S1D). Thus, PHD2 interacts with PP2A specifically through B55α.

We then assessed the effect of this interaction on PHD2 activity with respect to HIF1α stabilization. Co-expression of B55α prevented the degradation of HIF1α induced by $PHD2^{WT}$ but failed to regulate the activity of $PHD2^{S125A}$, indicating that PP2A/B55α acts specifically on S125 (Figure S1E). Only PHD2, but not PHD1 or PHD3, activity was increased by the administration of the PP2A inhibitor LB100, pointing to the specific relevance of this post-translational modification for PHD2 but not for the other family members (Figure S1F). Supporting the inhibitory effect of PP2A/B55α on PHD2-mediated HIF1α degradation, silencing of B55α in HEK293T cells could reduce the levels of wild-type HIF1α, but it did not have any effect on the HIF1α mutant (HIF1α-PP and also $HIF1α^{P402A/P564G}$), where P402 and P564 (normally hydroxylated by PHD2) were replaced by alanine and glycine, respectively (Figure 2F; Table S3). Proving the direct effect of PP2A/B55α on PHD2 phosphorylation, B55α overexpression could reduce the phosphorylation of $PHD2^{WT}$ on S125, whereas phosphorylation of $PHD2^{S125A}$ was undetectable under these conditions (Figure 2G; Table S3). A phosphatase assay showed that PP2A/B55α induced dephosphorylation of a PHD2-derived peptide in S125 (or of a standard peptide used as a positive control) but not of the mutated form (Figure 2H). This reaction was prevented by the PP2A inhibitor okadaic acid (OA) (Figure 2H). To confirm this observation, recombinant $PHD2^{WT}$ was dephosphorylated at S125 in the presence of purified B55α-containing PP2A complex (Figures 2I and 2J; Table S3). Similarly, phosphorylation of endogenous PHD2 was increased by silencing of B55α and decreased by silencing of P70S6K (Figure 2K), whereas total PHD2 levels were not affected (Figure 2L; Table S3). Altogether, these data demonstrate that PHD2 is dephosphorylated on S125 by PP2A/B55α and phosphorylated by the kinase P70S6K.

Release of PP2A/B55α Activity in Hypoxia Leads to PHD2 Dephosphorylation and Enhanced HIF1α Accumulation and Activity

To understand the relevance of PHD2 dephosphorylation in hypoxia, we exposed HT29 and DLD1 cells to low oxygen tensions; i.e., 1%, a concentration that still allows HIF hydroxylation by PHD2 (Berra et al., 2003; Figures 3A and 3B; Table S4). Under this condition, B55α knockdown prevented hypoxic HIF1α accumulation and activity in a PHD2-dependent manner (Figures 3A–3C; Table S4). Vice versa, degradation of HIF1α or Luc-ODDD in hypoxia could be achieved by overexpressing PHD2, but this process was prevented by co-expression of exogenous B55α (Figures S2A and S2B). These data demonstrate that, in hypoxia, PP2A/B55α contributes to HIF1α stabilization by dephosphorylating PHD2. Indeed, in a time-course fashion, we show that the peak of HIF1α occurs earlier in the presence of B55α than in its absence (Figure 3D) and that this event is associated with dephosphorylation of endogenous PHD2 already after exposure to hypoxia for 4 hr and, more robustly, at 16 hr (Figure 3E). Of interest, this dephosphorylation correlates with a progressive increase of PP2A activity, strongly reduced by siB55α or OA as control (Figure 3F). These data indicate a hypoxic molecular flow that, starting from the increase in PP2A/B55α activity, allows the decrease in PHD2 phosphorylation and, thus, HIF1α stabilization. Noteworthy is that, along the same time course, a progressive decrease of phosphorylated P70S6K occurs, partly antagonized by siB55α (Figure 3D). To further ascertain the temporal link between mTOR and P70S6K and PP2A, HIF1α accumulation was analyzed following reactivation of the mTOR pathway by silencing the hypoxia-induced mTOR inhibitor REDD1 (Brugarolas et al., 2004; Sofer et al., 2005). REDD1 silencing reduced HIF1α levels under hypoxic conditions, confirming that inhibition of mTOR signaling in hypoxia is favoring HIF1α stabilization (Figure 3G). B55α silencing also reduced HIF1α accumulation, and combination of both REDD1 and

(I and J) In vitro dephosphorylation assay where FLAG-PHD2 isolated from HEK293T cells was incubated alone or with immune-purified FLAG-B55α in dephosphorylation buffer (J). The anti-FLAG immunoprecipitation performed to isolate B55α shows the presence of PP2A/A and PP2A/C in the immunocomplexes (I). The phosphorylation status of PHD2 was detected by WB using a phospho-specific antibody (phospho-S125).

(K and L) DLD1 cells were transfected with siCTRL, or siB55α, or siP70S6K in triplicate. Total proteins were extracted, and liquid chromatography (LC)/MS was performed. Phosphorylated and non-phosphorylated PHD2 were absolutely quantified using parallel-reaction monitoring (PRM) and stable isotope-labeled (SIL) reference peptides of known concentrations (K). WB of the samples was performed as a control (L).

All WBs and immunoprecipitations were repeated three times on independent biological replicates. The graphs show mean ± SEM. See also Figure S2.

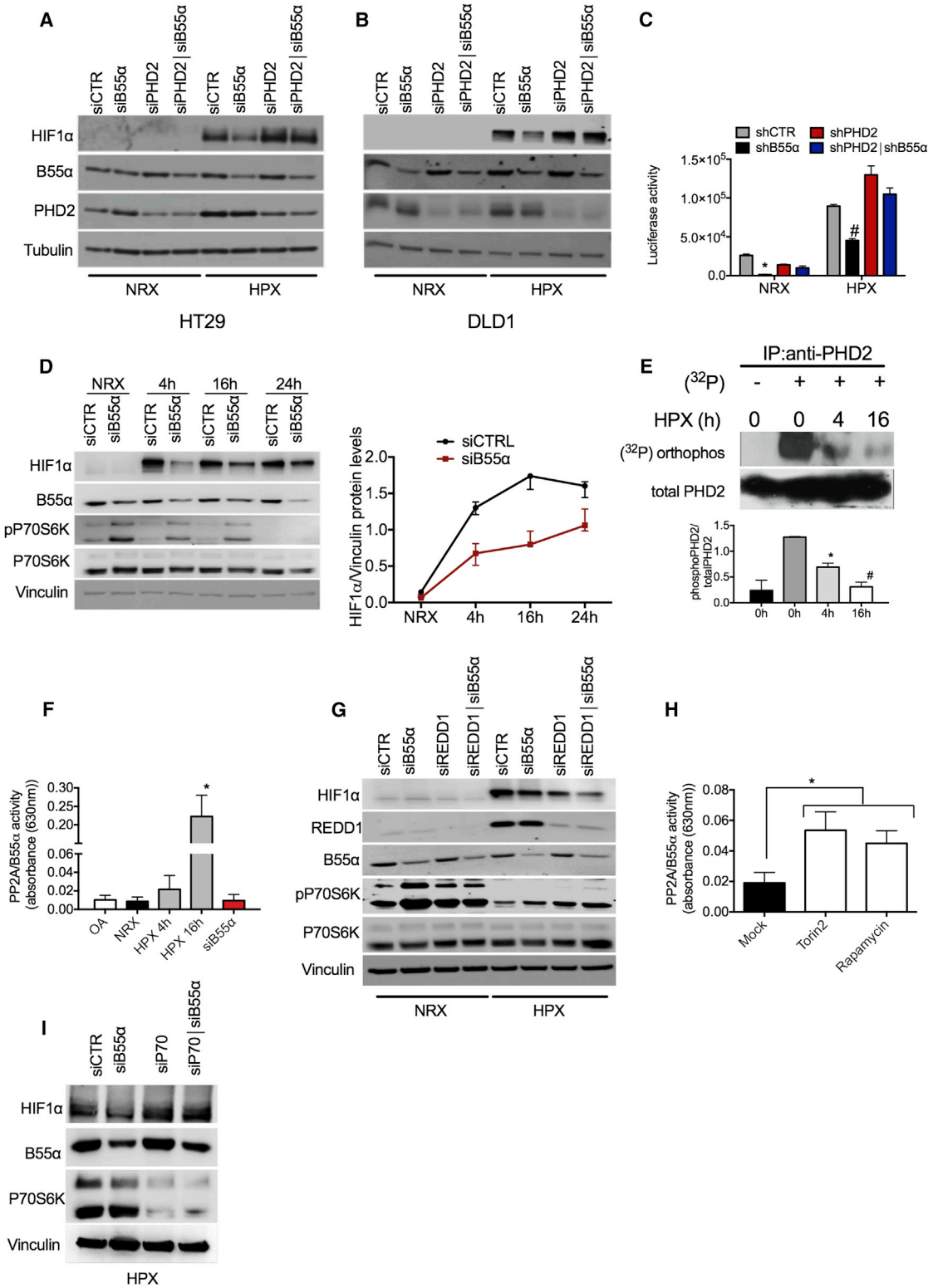

Figure 3. Hypoxia Blocks mTOR and Releases PP2A/B55α Activity to Dephosphorylate PHD2 and Increase HIF1α Protein Levels and Activity

(A and B) HT29 (A) or DLD1 (B) cells were transiently transfected with siCTR. siB55α, or siPHD2, alone or in combination. After 24 hr, cells were incubated either in normoxia (NRX, 21% O_2) or hypoxia (HPX, 1% O_2) for 16 hr, and WCEs were analyzed by WB.

(legend continued on next page)

B55α knockdown had an additive effect (Figure 3G), supporting the idea that inhibition of mTOR/P70S6K-mediated PHD2 phosphorylation and activation of B55α are simultaneous events, both required for full accumulation of HIF1α in hypoxia.

Next we investigated the mechanism(s) underlying PP2A activation. Several reports have shown that mTOR blockade releases PP2A activity (Cianfanelli et al., 2015; Hartley and Cooper, 2002; Peterson et al., 1999), and it is widely accepted that the mTOR pathway is inhibited by hypoxia (Sofer et al., 2005). Accordingly, our experiments showed progressive P70S6K deactivation in hypoxia (Figure 3D). We therefore measured PP2A/B55α activity in the presence of the mTOR blockers Torin2 or Rapamycin. Consistent with our hypothesis, we could observe a great increase in PP2A activity with both inhibitors (Figure 3H). Conversely, reactivation of mTOR signaling in hypoxia by REDD1 silencing prevented the activation of PP2A (Figure S2C). To further ascertain the involvement of P70S6K in this loop, we analyzed the effect of P70S6K or B55α silencing alone or in combination. Because activation of P70S6K was nearly abolished after 24 hr of hypoxic conditions (Figure 3D), experiments were performed at 4 hr of hypoxia; silencing of P70S6K or B55α oppositely regulated HIF1α levels, as already previously observed. Interestingly, combined P70S6K and B55α knockdown caused a further increase in HIF1α, indicating that silencing of P70S6K prevails over the loss of B55α/PP2A activity (Figure 3I). In summary, inactivation of the mTOR/P70S6K pathway by REDD1/hypoxia leads to increased PP2A function, PHD2 dephosphorylation, and, thus, HIF1α stabilization.

HIF1α Stabilization by PP2A/B55α Promotes Colorectal Cancer Cell Survival via Autophagy in a PHD2-Dependent Manner

In hypoxia, HIF1α stabilization promotes cancer cell survival by initiating autophagy, a process that requires transcriptional induction of BNIP3 and BNIP3L, leading to tumor progression (Mazure and Pouysségur, 2009). We thus speculated that PHD2 regulation by B55α might somehow modify cell viability in normoxia and/or in hypoxia. To explore this possibility, DLD1 cells stably knocked down for PHD2 or B55α, alone or in combination, were exposed to 21% or 1% oxygen. When exposed to hypoxia, cells depleted for B55α showed a significant increase in cell death compared with control cells, as assessed by measuring terminal deoxynucleotidyl transferase dUTP nick end labeling (TUNEL) staining or cleaved Poly(ADP-ribose) polymerase (PARP). Simultaneous depletion of PHD2 was able to rescue the increased cell death, indicating that B55α requires PHD2 to elicit its effect (Figures 4A and 4B; Table S5). The proliferation rate and cell cycle were both comparable under all conditions tested, either normoxia or hypoxia (Figures S3A–S3C). We then wondered whether B55α could promote hypoxic cell survival via autophagy. Hypoxic exposure of DLD1 control cells for 16 hr induced the autophagy markers *BNIP3* and *BNIP3L*; however, B55α silencing prevented this upregulation. Concomitant depletion of PHD2 and B55α restored *BNIP3* and *BNIP3L* levels back to the control level, supporting the idea of a PHD2-dependent role of B55α in hypoxia-induced autophagy (Figures 4C and 4D). To assess the influence of B55α in this process, we measured the autophagic substrates p62 and LC3B, which are, respectively, degraded and induced during autophagy. Under hypoxia, p62 halved and LC3B doubled in control cells, but B55α knockdown partially prevented this process in a PHD2-dependent manner (Figure 4E; Figure S3D; Table S5). To assess the link between autophagy and survival in hypoxia, DLD1 cells were silenced for B55α, for the autophagy-mediator Atg5 (Pyo et al., 2005), or for both (Figures S3E and S3F). In hypoxia, each silencing alone caused increased cell death and a reduction in LC3-II levels compared with the control, but combined knockdown of B55α and Atg5 was not synergic, suggesting that B55α exerts its mechanism of action on the same pathway of Atg5 (Figure 4F; Figure S3G).

To assess whether the effect of B55α knockdown on hypoxia-induced autophagy was mediated by a reduction in HIF1α levels, B55α-silenced and control cells were stably transfected with $HIF1\alpha^{P402A/P564G}$, a HIF1α double proline mutant insensitive to PHD-dependent degradation (Figure 4G; Table S5). As above, exposure to hypoxia promoted cell survival in control cells but much less in B55α-silenced cells; this phenotype was rescued upon concomitant overexpression of $HIF1\alpha^{P402A/P564G}$ (Figure 4H). Consistently, $HIF1\alpha^{P402A/P564G}$ overexpression also rescued the decrease in LC3-II levels observed upon B55α

(C) DLD1 cells were stably silenced for control, B55α, PHD2, or both (shCTR, shB55α, shPHD2, and shPHD2|shB55α, respectively). These cells were then transiently transfected with a hypoxia-response element (HRE)-Luc reporter and incubated for 16 hr in normoxia or hypoxia. Cells were then lysed, and luciferase activity was measured and normalized for protein concentration.

(D) WB of DLD1 cells transiently transfected with siCTR siB55α and incubated in normoxia or in hypoxia for the indicated time. The graph represents quantification of three independent experiments.

(E) DLD1 cells were incubated in normoxia or hypoxia for the indicated time in the presence of a phosphate-free medium containing 1 mCi of [^{32}P]orthophosphoric acid (NEN)/mL. WCEs were collected and immunoprecipitated with anti-PHD2 antibody. After blotting, the membrane was exposed to a Kodak phosphor imaging screen overnight. The graph shows the quantification and mean of two independent experiments.

(F) Measurement of the enzymatic activity of PP2A/B55α from WCEs of DLD1 cells incubated in normoxia (CTRL) and hypoxia for the indicated time or transfected with siB55α and incubated in hypoxia for 16 hr. OA and silencing of B55α siB55α were used as negative controls.

(G) WB of DLD1 cells transiently transfected with siCTR, siB55α, or REDD1 (siREDD1) alone or in combination and incubated either in normoxia or hypoxia for 16 hr.

(H) Measurement of the enzymatic activity of PP2A/B55α from WCE of DLD1 cells untreated (Mock) or incubated with 200 nM Torin2 and 1 μM Rapamycin for 16 hr.

(I) HEK393T cells were transfected with siCTR, siB55α, or siP70, alone or in combination. After 16 hr, cells were exposed to hypoxia for 4 hr, and WCEs were analyzed by WB.

All WBs were repeated three times on independent biological replicates. *$p < 0.05$ versus all other conditions under NRX in (C), versus 0 hr + ^{32}P in (E), versus all conditions in (F), and versus Mock in (H); #$p < 0.05$ versus all other conditions under HPX in (C) and versus 0 hr and 4 hr + ^{32}P in (E). The graphs show mean ± SEM. See also Figure S2.

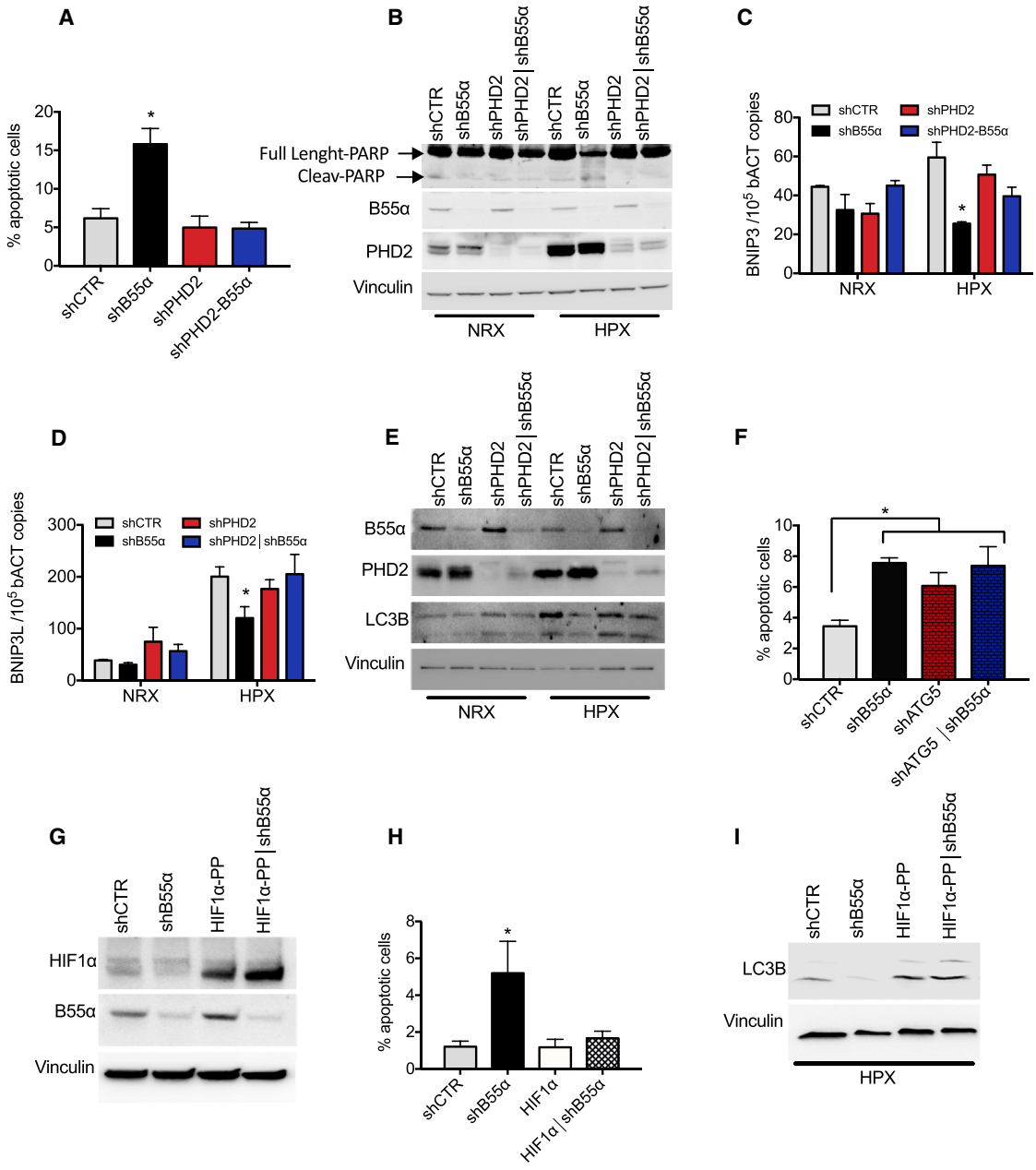

Figure 4. Silencing of B55α Induces Increased Apoptosis in Hypoxia in a PHD2-Dependent Manner

(A and B) DLD1 cells stably silenced for control, B55α, PHD2, or both (shCTR, shB55α, shPHD2, and shPHD2|shB55α, respectively) were cultured in normoxia or hypoxia for 96 hr (A) or 72 hr (B). Apoptosis was assessed by TUNEL staining (ApopTag) (A) or PARP cleavage (B).

(C and D) DLD1 cells stably silenced as in (A) were cultured in normoxia and in hypoxia for 16 hr. BNIP3 (C) and BNIP3L (D) mRNA levels were assessed by qRT-PCR.

(E) DLD1 cells stably silenced as in (A) were cultured in normoxia or hypoxia for 48 hr, and WCEs were analyzed by WB.

(F) DLD1 cells stably silenced for control, B55α, Atg5, or both (shCTR, shB55α, shAtg5, and shAtg5|shB55α, respectively) were cultured in normoxia or hypoxia for 96 hr. Apoptosis was assessed by TUNEL staining.

(G–I) DLD1 cells stably silenced for control (shCTR) or B55α (shB55α) were transduced with lentiviral vectors to stably express an empty vector or a hydroxylation-insensitive HIF1α (HIF1α-PP) (G). The cells were then cultured in normoxia or hypoxia for 96 hr, and apoptosis was assessed by TUNEL staining (H). The same cells were exposed to hypoxia for 48 hr, and WCEs were analyzed by WB (I).

All WBs were repeated three times on independent biological replicates. *$p < 0.05$ versus all other conditions in (A), (C), (D), and (H) and versus shCTR in (F). The graphs show mean ± SEM. See also Figure S3.

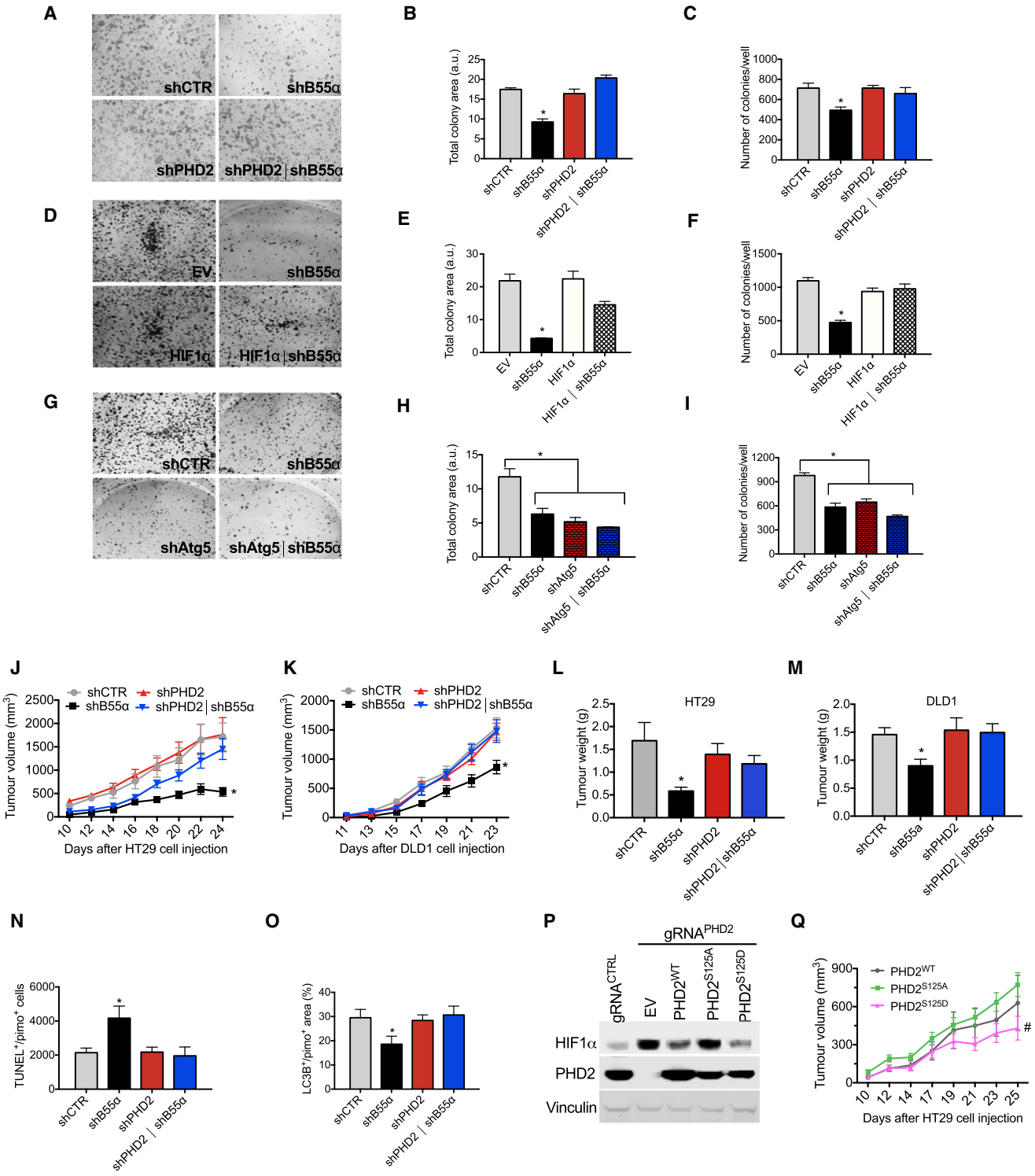

Figure 5. PP2A/B55α Promotes Colorectal Cancer Growth in a PHD2-Dependent Manner

(A–I) Focus formation assay with DLD1 cells stably silenced for control, B55α, PHD2, or both (shCTR, shB55α, shPHD2, and shPHD2|shB55α, respectively) (A–C), with DLD1 shCTR and shB55α stably transduced with an empty vector or a hydroxylation-insensitive HIF1α (EV, shB55α, HIF1α, and shB55α|HIF1α) (D–F), or with DLD1 cells stably silenced for control, B55α, Atg5 or both (shCTR, shB55α, and shAtg5, shAtg5|shB55α, respectively) (G–I). Representative images from one of three independent experiments are shown (A, D, and G). The graphs show the size (B, E, and H) and total number (C, F, and I) of colonies per well.

(legend continued on next page)

depletion (Figure 4I; Table S5). Thus, the pro-apoptotic effect seen after B55α silencing is dependent on a decrease in HIF1α levels because of sustained PHD2 activity under hypoxia.

PP2A/B55α Promotes Colorectal Cancer Growth in a PHD2-Dependent Manner

To elucidate the meaning of the B55α-PHD2 axis on tumorigenesis, we performed a focus-forming assay and a soft agar assay reflecting, respectively, the ability of cancer cells to bypass contact inhibition and to grow in the absence of adhesion. In both assays, uncontrolled growth led to increased oxygen consumption (Figure S4A; Leontieva et al., 2014). B55α silencing resulted in a significant reduction in colony size and number compared with the scrambled control and to PHD2 silencing (Figures 5A–5C; Figures S4B–S4D). This effect was rescued when B55α and PHD2 were concomitantly knocked down (Figures 5A–5C; Figures S4B–S4D), confirming that B55α works as a negative modulator of PHD2. Overexpression of undegradable $HIF1\alpha^{P402A/P564G}$ abrogated the decrease in colony size and density caused by B55α knockdown but did not affect the growth of control cells (Figures 5D–5F). To link the reduction in focus formation to impairment of the autophagic pathway, we measured colony size and numbers following single or combined knockdown of B55α and Atg5. Each silencing was equally effective in inhibiting colony formation, but the combined knockdown of B55α and Atg5 was not synergic, suggesting that autophagy-induced cancer cell survival by B55α unleashes its tumorigenic potential (Figures 5G–5I).

In vivo, silencing of B55α in DLD1 or HT29 cells subcutaneously injected into nude mice resulted in the formation of smaller tumors. This effect was PHD2-dependent because concomitant silencing of PHD2 prevented it, whereas PHD2 knockdown alone did not affect cancer growth (Figures 5J–5M). In line with our in vitro experiments, compared with the control, cell death and autophagy in the hypoxic (pimonidazole-positive) niches of the tumor were, respectively, increased and reduced upon B55α silencing but rescued by combined knockdown of B55α and PHD2; PHD2 silencing alone did not affect either parameters (Figures 5N and 5O). Conversely, cancer cell proliferation was not significantly affected (Figure S4E). In addition, stromal component such as leukocyte infiltration and blood vessel density were similar under all experimental conditions (Figures S4F and S4G). Overall, these findings indicate that PP2A/B55α plays a pro-tumoral role by inactivating PHD2.

By using CRIPSR/Cas9, we generated PHD2 KO HT29 cells (Figure S4H) that were then reconstituted with either $PHD2^{WT}$, $PHD2^{S125A}$, or $PHD2^{S125D}$. These cell lines showed different levels of HIF1α according to our previous in vitro data, with $PHD2^{S125A}$ and $PHD2^{S125D}$ being, respectively, less and more active than the wild-type isoform (Figure 5P). In vivo, HT29 cells expressing PHD^{2S125D} showed a significant reduction in tumor growth compared with cells expressing $PHD2^{S125A}$; $PHD2^{WT}$-expressing cells displayed, instead, an intermediate phenotype (Figure 5Q). In sum, $PHD2^{S125D}$ mutant mimics B55α silencing, both of which have an antitumor effect.

Finally, we collected tumor tissues and normal counterparts from CRC patients, and B55α, HIF1α, and REDD1 protein levels were analyzed by western blot. Compared with normal colon, all tumor samples displayed increased protein levels of HIF1α, B55α, and REDD1 (Figures 6A–6D). Importantly, targeted mass spectrometry revealed that the fraction of phospho-S125 in cancerous colon tissue was about 60% decreased compared with healthy colon (Figure 6E; Figures S5A and S5B). Consistent with the induction of PHD2 by HIF1 itself (Fong and Takeda, 2008), the total amount of PHD2 was slightly higher in the tumor compared with normal tissue, although this difference did not reach significance (Figure 6F). Overall, these observations highlight the relevance of B55α-PP2A signaling in the regulation of PHD2 phosphorylation and HIF1α accumulation in CRC.

According to our model, it follows that, subsequent to an mTOR block in hypoxia, not only the phosphorylation of PHD2 by P70S6K is inhibited but PP2A/B55α activity is also liberated (Hartley and Cooper, 2002; Peterson et al., 1999; Roberts et al., 2014). Interestingly, B55α silencing prevents P70S6K inactivation, indicating that the phosphorylation and dephosphorylation machineries of PHD2 are mutually exclusive. As a consequence, increased dephosphorylation on S125 results in impaired enzymatic activity of PHD2. Consequently, HIF1α accumulates and favors cancer cell survival and tumor growth (Figure 6G).

DISCUSSION

PHD2 is the main regulator of HIF1α, one of the key responders to hypoxia, and broadly expressed in tumors (Keith et al., 2011). Although it is generally accepted that oxygen is the most important determinant of PHD2 activity, here we investigate the possible involvement of oxygen-independent, post-translational modification of PHD2. We find that the phosphorylation status of PHD2 is important for efficient control of HIF1 levels. The kinase P70S6K and the phosphatase PP2A/B55α directly phosphorylate and dephosphorylate PHD2 on S125. When S125 is mutated

(J and K) In vivo growth curves of xenograft tumors derived by subcutaneous injection in nude mice of HT29 (J) or DLD1 (K) cells stably silenced for control, B55α, PHD2, or both (shCTR, shB55α, shPHD2, and shPHD2|shB55α, respectively).
(L and M) Tumor weights of HT29 (L) or DLD1 (M) cells 24 or 23 days after tumor cell injection, respectively.
(N) Morphometric quantification of DLD1 tumor sections stained for ApopTag showing apoptosis in the PIMO-positive area of the tumor.
(O) Morphometric quantification of DLD1 tumor sections stained for LC3 and PIMO, showing autophagy in hypoxic areas of the tumor. The data combine two or three independent experiments using seven or eight mice per condition in each experiment.
(P) WB analysis for HIF1α and PHD2 from control HT29 (guide RNA $[gRNA]^{CTRL}$) and HT29 cells knocked out for PHD2 by means of a $gRNA^{PHD2}$ and then reconstituted with a lentiviral vector encoding $PHD2^{WT}$, $PHD2^{S125A}$, and $PHD2^{S125D}$ or an EV.
(Q) In vivo growth curve of xenograft tumors derived by subcutaneous injection into nude mice of PHD2 knockout HT29 cells ($gRNA^{PHD2}$) stably expressing $PHD2^{WT}$, $PHD2^{S125A}$, and $PHD2^{S125D}$. The data combine two independent experiments using six mice per condition in each experiment. The WB was repeated twice.
*$p < 0.05$ versus all other conditions; #$p < 0.05$ versus $PHD2^{S125A}$. The graphs show mean ± SEM. See also Figure S4.

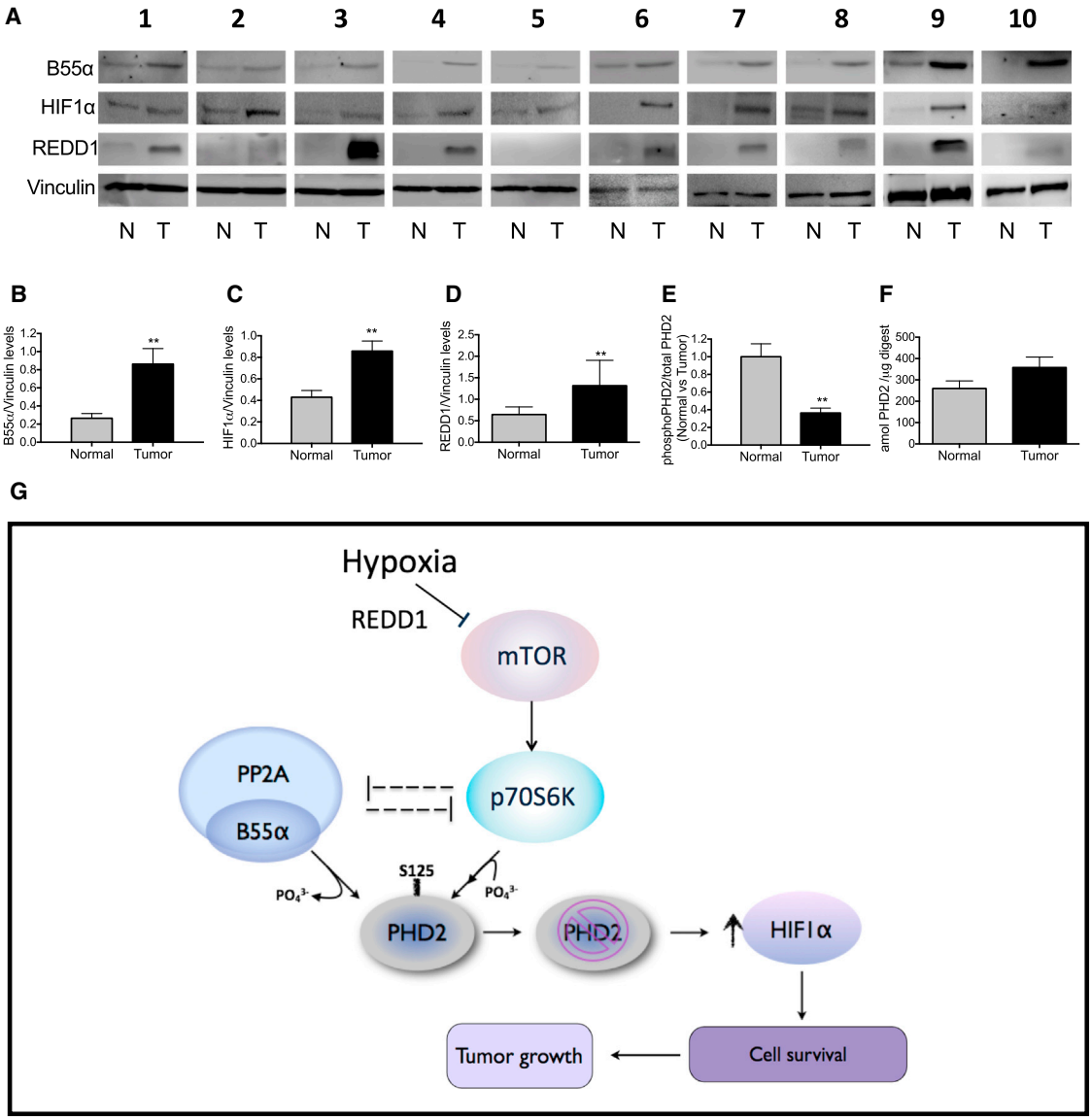

Figure 6. Evidence of the B55α-PHD2-HIF1α Axis in Colorectal Cancer Patients

(A–D) WB analysis (A) and quantification of B55α (B), HIF1α (C) and REDD1 (D) protein levels in normal or tumor colorectal cancer tissues from ten colorectal cancer patients. Vinculin was used as a loading control.

(E and F) LC/MS-based quantification of phosphorylated S125 over total PHD2 ratios in healthy versus colorectal cancer tissues using targeted PRM and SIL reference peptides. The fraction of S125 phosphorylation on total PHD2 in healthy tissue is normalized to 1 (E). Total PHD2 levels are shown in (F). **$p < 0.01$ versus the other condition. The graphs show mean ± SEM. See also Figure S5.

(G) Schematic of the pathways controlling the phosphorylation status of PHD2 on S125 and the levels of HIF1α. The mTOR downstream kinase P70S6K is responsible for the direct phosphorylation of PHD2. Instead, PP2A/B55α is responsible for the direct dephosphorylation, leading to a partial inactivation of PHD2 even when oxygen is not limiting. In hypoxia, the mTOR pathway is inhibited, and, as a consequence, PP2A/B55α activity is liberated. It follows that P70S6K is blocked by both PP2A and by the inhibition of mTOR. The enzymatic release of PP2A/B55α and the inhibition of P70S6K lead to complete dephosphorylation of PHD2 on S125, resulting in the overall reduction of its activity and accumulation of HIF1α. After stabilization, HIF1α promotes hypoxic cell survival via autophagy and fosters tumor growth.

to alanine, PHD2 shows an impaired ability to degrade HIF1α or an ODDD luciferase fusion protein, which is associated with a reduction of OH-HIF1α, indicating a crucial role of S125 phosphorylation in modulating PHD2 activity.

The mechanism by which this phosphorylation modifies PHD2 activity remains to be elucidated. Indeed, S125 is a residue located at the N terminus of the protein and does not involve its catalytic domain. Moreover, although others have shown that phosphorylation on PHD1 S130 by CDK1 affects the binding affinity of PHD1 for HIF1α (Ortmann et al., 2016), the phosphorylation status of PHD2 on S125 does not affect the interaction between PHD2 and HIF1α (data not shown). Therefore, this

phosphorylation site might be relevant for the affinity of PHD2 for oxygen and/or cosubstrates or for other partners, such as LIMD1 or von Hippel-Lindau (VHL) (Foxler et al., 2012).

In hypoxia, mTOR inhibition prohibits P70S6K activity, which, in turn, unleashes PP2A/B55α signaling. The downregulation of P70S6K, a kinase targeting PHD2, and the mutual upregulation of PP2A/B55α phosphatase activity lead to dephosphorylation and partial inactivation of PHD2, ultimately promoting HIF1α stabilization (Figure 6G). These data therefore indicate a hypoxic regulatory flow that starts with downregulation of P70S6K activity and moves to the activation of PP2A/B55α. The combined action of these processes potentiates/accelerates the inactivation of PHD2 during hypoxia, leading to HIF1α stabilization. Furthermore, HIF1α, by promoting REDD1 transcription (Brugarolas et al., 2004), contributes to mTOR inactivation, thus enforcing a positive feedback loop that promotes survival of hypoxic tumor cells.

With these data, we add a further piece to the crosstalk between mTOR and HIF1α. It has been reported that the mTOR pathway controls HIF1α protein synthesis in normoxia (Brugarolas et al., 2004; Hudson et al., 2002). Here we explain how HIF1α can be stabilized under low oxygen availability or nutrient starvation (Nishimoto et al., 2014), two conditions that turn off the mTOR pathway. Accordingly, REDD1 blockade and subsequent mTOR activation have been linked to an antitumoral response, and REDD1 overexpression has been described in CRC as well as in several other tumor types (Chang et al., 2009; Jia et al., 2014; Kucejova et al., 2011) (http://www.cbioportal.org/). It is reasonable that these tumors are highly hypoxic, and REDD1 overexpression upregulates hypoxia-induced genes (Brugarolas et al., 2004). In the opposite scenario, in normoxic cells, active mTOR/P70S6K increases HIF1α translation, but PHD2 activity is promoted as well so that, ultimately, excessive HIF activation is prevented.

According to our model, HIF1α stabilization by PP2A will initiate an adaptive response, allowing cells to survive the hostile conditions that characterize the tumor microenvironment (Keith et al., 2011). Although autophagy in cancer has been associated with opposing functions (Mathew et al., 2007; Shchors et al., 2015), autophagy in CRC cells has been shown to be pro-survival following amino acid starvation (Sato et al., 2007). Here we demonstrate that hypoxia is able to trigger autophagic survival through stabilization of HIF1α levels, which requires PHD2 dephosphorylation by PP2A/B55α. In this way, the protective role of HIF1α is cell-autonomous and not due to the indirect effect of this pathway on the tumor stroma, such as via vascular endothelial growth factor (VEGF) production and blood vessel formation (Tsuzuki et al., 2000). However, prolonged activation of the autophagic process would lead to excessive self-eating with consequent induction of cell death (Liu and Levine, 2015). Transcriptional induction of PHD2 upon chronic hypoxia (Epstein et al., 2001) will overrule the inhibition of PHD2 by PP2A, bringing HIF1α to lower levels and turning off autophagy. In this scenario, a post-translational modification represents the fastest way for the cell to survive.

It has already been shown that B55α is induced in cancer cells at both the transcript and protein levels when the key metabolite glutamine becomes limited or upon DNA damage (Kalev et al., 2012). The ability of B55α silencing to abate the neoplastic features of HT29 and DLD1 cells in vitro and in vivo indicates that B55α can have a pro-survival, tumor-promoting role in colorectal cancer, supported by our study in a small cohort of CRC patients and by recent data showing that, of all the B subunits, only B55α is specifically upregulated in CRC human samples (Gilan et al., 2015). Another study has reported a significant association between expression of HIF1α and CRC staging, involvement of lymph nodes, and liver metastases, resulting in an inverse correlation between HIF1α levels and overall survival (Cao et al., 2009). Because we have shown that HIF1α levels positively correlate with B55α because of its negative modulation of PHD2, we suggest that targeting B55α might serve as a promising therapeutic approach for CRC, especially to tackle tumors overexpressing HIF1α. So far, the pan-PP2A inhibitor okadaic acid has been shown to promote tumor growth and is associated with adverse reactions (Bialojan and Takai, 1988). This is due to the pleiotropic and multifunctional role of 100 combinations of the PP2A holoenzyme. Based on our observation, we speculate that a molecule capable of blocking B55α or, even more specifically, the interaction between B55α and PHD2, might display higher selectivity with an univocal anti-tumor effect and, likely, lower toxicity.

At this stage, our study provides insights into how, in the context of CRC, a specific post-translational modification of PHD2 can promptly activate a survival response by controlling HIF1α in an oxygen-independent manner, thus extending the role of PHD2 beyond its initially recognized function as an oxygen sensor.

EXPERIMENTAL PROCEDURES

More detailed methods can be found in the Supplemental Experimental Procedures.

Cell Culture and Transfections

HEK293T, DLD1, and HT29 cell lines were routinely cultured in DMEM (Gibco) supplemented with 10% heat-inactivated fetal bovine serum (FBS, Gibco), 2 mM glutamine (Life Technologies), and 100 units/mL penicillin and 100 μg/mL streptomycin (Life Technologies). Cells were maintained in a humidified incubator at 37°C and 5% CO_2. For hypoxia experiments, cells were incubated in a hypoxic glovebox (37°C, 5% CO_2, 1% O_2) for the indicated times. Transfections were performed with Lipofectamine 2000 transfection reagent or Lipofectamine RNAiMax (Life Technologies) according to the manufacturer's instructions.

Phosphatase Assay

Phosphatase assays were performed by using DuoSet IC-human/mouse/rat active PP2A (R&D Systems) according to the manufacturer's instructions. 100 μg of whole-cell extract from DLD1 cells was added to PP2A antibody-coated wells. Recombinant PHD2 peptide (amino acids [aa] 113–130) synthetized by Pepscan and the positive control (serine/threonine phosphatase substrate I, part 842098) were used as phosphatase substrates.

Kinase Assay

The purified wild-type or mutant PHD2-FLAGM2 proteins (100 ng) were incubated in kinase buffer (25 mM 3-Morpholinopropane-1-sulfonic acid (MOPS) [pH 7.2], 25 mM $MgCl_2$, 5 mM EGTA, 2 mM EDTA, 250 μM DTT, and 6 mM β-glycerophosphate) in the presence of active P70S6K (4 ng/μL, SignalChem), 250 μM ATP, and 2 μCi γ-^{32}P-ATP (PerkinElmer). After 20-min incubation at 30°C, samples were denaturated by incubating with 4× SDS sample buffer at 95°C for 10 min and separated by 10% SDS-PAGE. Thereafter, the gel was blotted onto a nitrocellulose membrane, and the membrane was exposed to a Kodak phosphor imaging screen overnight. Autoradiography was

detected with MolecularImager FX using Quantity One software (all from Bio-Rad). Afterward, the total proteins were detected by using an antibody against PHD2.

Focus Formation and Soft Agar Assay

For the focus formation assay, DLD1 cells were plated at 2×10^3 cells/well on a 6-well cell culture plate and cultured for 10 days. The cultured cells were stained and fixed with 0.5% crystal violet in a fixating solution containing 10% acetic acid and 10% methanol in water. For the soft agar assay, 10^3 DLD1 cells were suspended in 2 mL of 0.5% (w/v) agar containing DMEM/10% fetal bovine serum on a 1% (w/v) agar solution in 24-well plates. Colonies appeared microscopically after 10 days and were visible to the naked eye after 15–20 days of incubation.

Xenograft Tumors

DLD1 and HT29 cells were harvested, and single-cell suspensions of $3 - 10^6$ cells in 200 μL of PBS were injected subcutaneously into the right flanks of nude mice. Tumor volumes were measured three times a week with a caliper and calculated using the following formula: $V = \pi \times [d^2 \times D] / 6$, where d is the minor tumor axis and D is the major tumor axis. All the experimental procedures were approved by the Institutional Animal Care and Research Advisory Committee of the KU Leuven.

CRC Patient Selection

For this study, ten patients diagnosed with CRC who underwent surgical resection were selected. This study was approved by the institutional ethical commission at the University Hospital of Leuven, Belgium.

Statistics

All statistical analyses were performed using GraphPad Prism software. Statistical significance was calculated by two-tailed unpaired t test on two experimental conditions or two-way ANOVA when more than two groups were compared, with $p < 0.05$ considered statistically significant. Western blots and immunoprecipitations are representative of three independent experiments. Focus formation assays, qRT-PCR, luciferase assays, and phosphatase assays are representative of three independent biological experiments where each experiment was done by three technical replicates. All graphs show mean values ± SEM.

SUPPLEMENTAL INFORMATION

Supplemental Information includes Supplemental Experimental Procedures, five figures, and five tables and can be found with this article online at http://dx.doi.org/10.1016/j.celrep.2017.01.051.

AUTHOR CONTRIBUTIONS

G.D.C. performed experimental design, all experiments, acquisition of data and analysis, and interpretation of all data and wrote the manuscript. S.T.C. performed the western blot experiments. S.L., R.P.Z., and A.S. performed the mass spectrometry (MS) analysis on cells and tumor samples. S.D. performed the initial interaction study by MS. M.D.M. designed the CRISPR/Cas9 experiment. M.E. performed the histological stainings and analysis. D.M. and T.K. performed the in vitro kinase assays. H.P. provided clinical samples. K.G. performed the MS on PHD2 to identify the phosphorylation sites. F.M. conducted scientific direction. M.M. performed experimental design, analyzed of data, conducted scientific direction, and wrote the manuscript.

ACKNOWLEDGMENTS

The authors thank B. Meeusen, G. Manzella, and J. Serneels for technical assistance and A. Sablina and T. Acker for sharing plasmids and reagents. This work was supported by grants from ERANET (OxyUC, G0D8115N), FWO (1505611N00), Stichting Tegen Kanker (2010-169), Bundesministerium für Bildung und Forschung, and the Ministerium für Innovation, Wissenschaft und Forschung des Landes Nordrhein-Westfalen. G.D.C. is supported by a Pegasus FWO-Marie Curie fellowship (1211413N), M.E. by DFG (EH 472/1-1), and S.D. by VLK (EVDS and 419.052.173). M.M. received an ERC starting grant (OxyMO, 308459).

Received: November 25, 2014
Revised: October 22, 2016
Accepted: January 19, 2017
Published: February 14, 2017

REFERENCES

Appelhoff, R.J., Tian, Y.M., Raval, R.R., Turley, H., Harris, A.L., Pugh, C.W., Ratcliffe, P.J., and Gleadle, J.M. (2004). Differential function of the prolyl hydroxylases PHD1, PHD2, and PHD3 in the regulation of hypoxia-inducible factor. J. Biol. Chem. *279*, 38458–38465.

Berra, E., Benizri, E., Ginouvès, A., Volmat, V., Roux, D., and Pouysségur, J. (2003). HIF prolyl-hydroxylase 2 is the key oxygen sensor setting low steady-state levels of HIF-1alpha in normoxia. EMBO J. *22*, 4082–4090.

Bialojan, C., and Takai, A. (1988). Inhibitory effect of a marine-sponge toxin, okadaic acid, on protein phosphatases. Specificity and kinetics. Biochem. J. *256*, 283–290.

Brugarolas, J., Lei, K., Hurley, R.L., Manning, B.D., Reiling, J.H., Hafen, E., Witters, L.A., Ellisen, L.W., and Kaelin, W.G., Jr. (2004). Regulation of mTOR function in response to hypoxia by REDD1 and the TSC1/TSC2 tumor suppressor complex. Genes Dev. *18*, 2893–2904.

Cao, D., Hou, M., Guan, Y.S., Jiang, M., Yang, Y., and Gou, H.F. (2009). Expression of HIF-1alpha and VEGF in colorectal cancer: association with clinical outcomes and prognostic implications. BMC Cancer *9*, 432.

Chan, D.A., Sutphin, P.D., Yen, S.E., and Giaccia, A.J. (2005). Coordinate regulation of the oxygen-dependent degradation domains of hypoxia-inducible factor 1 alpha. Mol. Cell. Biol. *25*, 6415–6426.

Chang, B., Liu, G., Yang, G., Mercado-Uribe, I., Huang, M., and Liu, J. (2009). REDD1 is required for RAS-mediated transformation of human ovarian epithelial cells. Cell Cycle *8*, 780–786.

Cianfanelli, V., Fuoco, C., Lorente, M., Salazar, M., Quondamatteo, F., Gherardini, P.F., De Zio, D., Nazio, F., Antonioli, M., D'Orazio, M., et al. (2015). AMBRA1 links autophagy to cell proliferation and tumorigenesis by promoting c-Myc dephosphorylation and degradation. Nat. Cell Biol. *17*, 20–30.

De Bock, K., Mazzone, M., and Carmeliet, P. (2011). Antiangiogenic therapy, hypoxia, and metastasis: risky liaisons, or not? Nat. Rev. Clin. Oncol. *8*, 393–404.

Epstein, A.C., Gleadle, J.M., McNeill, L.A., Hewitson, K.S., O'Rourke, J., Mole, D.R., Mukherji, M., Metzen, E., Wilson, M.I., Dhanda, A., et al. (2001). C. elegans EGL-9 and mammalian homologs define a family of dioxygenases that regulate HIF by prolyl hydroxylation. Cell *107*, 43–54.

Fong, G.H., and Takeda, K. (2008). Role and regulation of prolyl hydroxylase domain proteins. Cell Death Differ. *15*, 635–641.

Foxler, D.E., Bridge, K.S., James, V., Webb, T.M., Mee, M., Wong, S.C., Feng, Y., Constantin-Teodosiu, D., Petursdottir, T.E., Bjornsson, J., et al. (2012). The LIMD1 protein bridges an association between the prolyl hydroxylases and VHL to repress HIF-1 activity. Nat. Cell Biol. *14*, 201–208.

Gilan, O., Diesch, J., Amalia, M., Jastrzebski, K., Chueh, A.C., Verrills, N.M., Pearson, R.B., Mariadason, J.M., Tulchinsky, E., Hannan, R.D., and Dhillon, A.S. (2015). PR55α-containing protein phosphatase 2A complexes promote cancer cell migration and invasion through regulation of AP-1 transcriptional activity. Oncogene *34*, 1340.

Ginouvès, A., Ilc, K., Macías, N., Pouysségur, J., and Berra, E. (2008). PHDs overactivation during chronic hypoxia "desensitizes" HIFalpha and protects cells from necrosis. Proc. Natl. Acad. Sci. USA *105*, 4745–4750.

Hartley, D., and Cooper, G.M. (2002). Role of mTOR in the degradation of IRS-1: regulation of PP2A activity. J. Cell. Biochem. *85*, 304–314.

Hudson, C.C., Liu, M., Chiang, G.G., Otterness, D.M., Loomis, D.C., Kaper, F., Giaccia, A.J., and Abraham, R.T. (2002). Regulation of hypoxia-inducible

factor 1alpha expression and function by the mammalian target of rapamycin. Mol. Cell. Biol. *22*, 7004–7014.

Jia, W., Chang, B., Sun, L., Zhu, H., Pang, L., Tao, L., Zou, H., Du, J., Dong, Y., Qi, Y., et al. (2014). REDD1 and p-AKT over-expression may predict poor prognosis in ovarian cancer. Int. J. Clin. Exp. Pathol. *7*, 5940–5949.

Jokilehto, T., and Jaakkola, P.M. (2010). The role of HIF prolyl hydroxylases in tumour growth. J. Cell. Mol. Med. *14*, 758–770.

Kalev, P., Simicek, M., Vazquez, I., Munck, S., Chen, L., Soin, T., Danda, N., Chen, W., and Sablina, A. (2012). Loss of PPP2R2A inhibits homologous recombination DNA repair and predicts tumor sensitivity to PARP inhibition. Cancer Res. *72*, 6414–6424.

Keith, B., Johnson, R.S., and Simon, M.C. (2011). HIF1α and HIF2α: sibling rivalry in hypoxic tumour growth and progression. Nat. Rev. Cancer *12*, 9–22.

Kucejova, B., Peña-Llopis, S., Yamasaki, T., Sivanand, S., Tran, T.A., Alexander, S., Wolff, N.C., Lotan, Y., Xie, X.J., Kabbani, W., et al. (2011). Interplay between pVHL and mTORC1 pathways in clear-cell renal cell carcinoma. Mol. Cancer Res. *9*, 1255–1265.

Leontieva, O.V., Demidenko, Z.N., and Blagosklonny, M.V. (2014). Contact inhibition and high cell density deactivate the mammalian target of rapamycin pathway, thus suppressing the senescence program. Proc. Natl. Acad. Sci. USA *111*, 8832–8837.

Liu, Y., and Levine, B. (2015). Autosis and autophagic cell death: the dark side of autophagy. Cell Death Differ. *22*, 367–376.

Mathew, R., Karantza-Wadsworth, V., and White, E. (2007). Role of autophagy in cancer. Nat. Rev. Cancer *7*, 961–967.

Mazure, N.M., and Pouysségur, J. (2009). Atypical BH3-domains of BNIP3 and BNIP3L lead to autophagy in hypoxia. Autophagy *5*, 868–869.

Nishimoto, A., Kugimiya, N., Hosoyama, T., Enoki, T., Li, T.S., and Hamano, K. (2014). HIF-1α activation under glucose deprivation plays a central role in the acquisition of anti-apoptosis in human colon cancer cells. Int. J. Oncol. *44*, 2077–2084.

Núñez-O'Mara, A., Gerpe-Pita, A., Pozo, S., Carlevaris, O., Urzelai, B., Lopitz-Otsoa, F., Rodríguez, M.S., and Berra, E. (2015). PHD3-SUMO conjugation represses HIF1 transcriptional activity independently of PHD3 catalytic activity. J. Cell Sci. *128*, 40–49.

Ortmann, B., Bensaddek, D., Carvalhal, S., Moser, S.C., Mudie, S., Griffis, E.R., Swedlow, J.R., Lamond, A.I., and Rocha, S. (2016). CDK-dependent phosphorylation of PHD1 on serine 130 alters its substrate preference in cells. J. Cell Sci. *129*, 191–205.

Pan, Y., Mansfield, K.D., Bertozzi, C.C., Rudenko, V., Chan, D.A., Giaccia, A.J., and Simon, M.C. (2007). Multiple factors affecting cellular redox status and energy metabolism modulate hypoxia-inducible factor prolyl hydroxylase activity in vivo and in vitro. Mol. Cell. Biol. *27*, 912–925.

Peterson, R.T., Desai, B.N., Hardwick, J.S., and Schreiber, S.L. (1999). Protein phosphatase 2A interacts with the 70-kDa S6 kinase and is activated by inhibition of FKBP12-rapamycinassociated protein. Proc. Natl. Acad. Sci. USA *96*, 4438–4442.

Pyo, J.O., Jang, M.H., Kwon, Y.K., Lee, H.J., Jun, J.I., Woo, H.N., Cho, D.H., Choi, B., Lee, H., Kim, J.H., et al. (2005). Essential roles of Atg5 and FADD in autophagic cell death: dissection of autophagic cell death into vacuole formation and cell death. J. Biol. Chem. *280*, 20722–20729.

Roberts, D.J., Tan-Sah, V.P., Ding, E.Y., Smith, J.M., and Miyamoto, S. (2014). Hexokinase-II positively regulates glucose starvation-induced autophagy through TORC1 inhibition. Mol. Cell *53*, 521–533.

Sato, K., Tsuchihara, K., Fujii, S., Sugiyama, M., Goya, T., Atomi, Y., Ueno, T., Ochiai, A., and Esumi, H. (2007). Autophagy is activated in colorectal cancer cells and contributes to the tolerance to nutrient deprivation. Cancer Res. *67*, 9677–9684.

Seshacharyulu, P., Pandey, P., Datta, K., and Batra, S.K. (2013). Phosphatase: PP2A structural importance, regulation and its aberrant expression in cancer. Cancer Lett. *335*, 9–18.

Shchors, K., Massaras, A., and Hanahan, D. (2015). Dual Targeting of the Autophagic Regulatory Circuitry in Gliomas with Repurposed Drugs Elicits Cell-Lethal Autophagy and Therapeutic Benefit. Cancer Cell *28*, 456–471.

Sofer, A., Lei, K., Johannessen, C.M., and Ellisen, L.W. (2005). Regulation of mTOR and cell growth in response to energy stress by REDD1. Mol. Cell. Biol. *25*, 5834–5845.

Stolze, I.P., Tian, Y.M., Appelhoff, R.J., Turley, H., Wykoff, C.C., Gleadle, J.M., and Ratcliffe, P.J. (2004). Genetic analysis of the role of the asparaginyl hydroxylase factor inhibiting hypoxia-inducible factor (FIH) in regulating hypoxia-inducible factor (HIF) transcriptional target genes [corrected]. J. Biol. Chem. *279*, 42719–42725.

Tsuzuki, Y., Fukumura, D., Oosthuyse, B., Koike, C., Carmeliet, P., and Jain, R.K. (2000). Vascular endothelial growth factor (VEGF) modulation by targeting hypoxia-inducible factor-1alpha–> hypoxia response element–> VEGF cascade differentially regulates vascular response and growth rate in tumors. Cancer Res. *60*, 6248–6252.

Cell Reports, Volume *18*

Supplemental Information

The mTOR and PP2A Pathways Regulate PHD2 Phosphorylation to Fine-Tune HIF1α Levels and Colorectal Cancer Cell Survival under Hypoxia

Giusy Di Conza, Sarah Trusso Cafarello, Stefan Loroch, Daniela Mennerich, Sofie Deschoemaeker, Mario Di Matteo, Manuel Ehling, Kris Gevaert, Hans Prenen, Rene Peiman Zahedi, Albert Sickmann, Thomas Kietzmann, Fabiola Moretti, and Massimiliano Mazzone

Supplemental Information

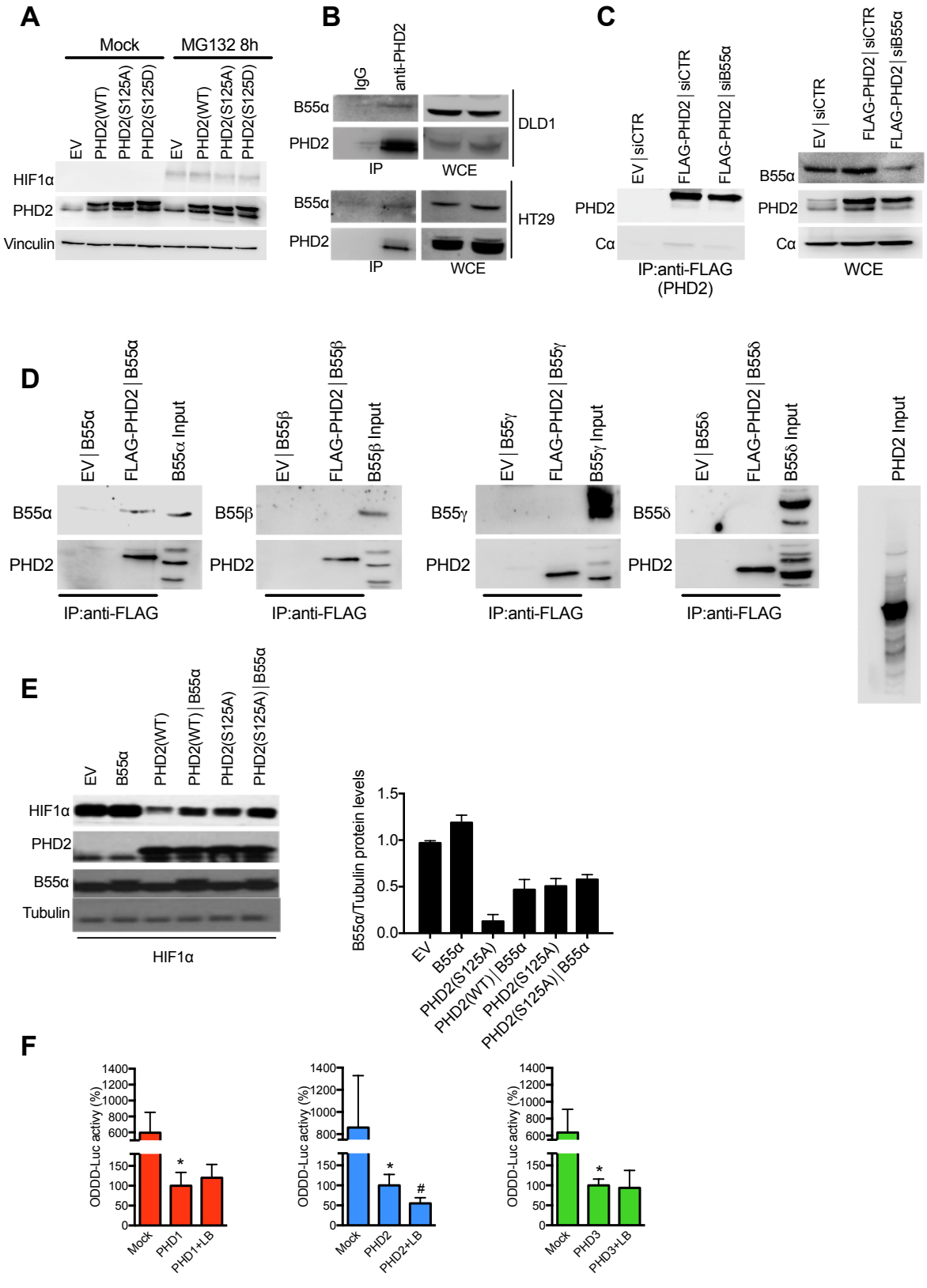
A
Mock
MG132 8h
EV
PHD2(WT)
PHD2(S125A)
PHD2(S125D)
HIF1α
PHD2
Vinculin
B
IgG
anti-PHD2
B55α
PHD2
IP
WCE
DLD1
HT29
C
EV | siCTR
FLAG-PHD2 | siCTR
FLAG-PHD2 | siB55α
Cα
IP:anti-FLAG
(PHD2)
WCE
D
EV | B55α
FLAG-PHD2 | B55α
B55α Input
EV | B55β
FLAG-PHD2 | B55β
B55β Input
EV | B55γ
FLAG-PHD2 | B55γ
B55γ Input
EV | B55δ
FLAG-PHD2 | B55δ
B55δ Input
PHD2 Input
B55β
B55γ
B55δ
IP:anti-FLAG
E
EV
B55α
PHD2(WT)
PHD2(WT) | B55α
PHD2(S125A)
PHD2(S125A) | B55α
Tubulin
HIF1α
B55α/Tubulin protein levels
1.5
1.0
0.5
0.0
F
ODDD-Luc activy (%)
1400
1200
1000
800
600
150
100
50
0
Mock
PHD1
PHD1+LB
PHD2
PHD2+LB
PHD3
PHD3+LB
*
#

Figure S1, related to Figure 1. PP2A/B55α specifically binds and dephosphorylates PHD2 in S125.
(A) HT29 cells were transfected with an empty vector (EV) or with PHD2 (WT, S125A or S125D). After 16 hours (h), cells were treated with the proteasome inhibitor MG132 (10μM) for 8h, lysed and analyzed by WB. (B) WCEs from DLD1 or HT29 cells were collected and immunoprecipitated with an anti-PHD2 antibody or with anti-IgG as control. Immunocomplexes with endogenous B55α were detected by WB analysis. (C) HEK293T cells transiently silenced for control (siCTR) or B55α (siB55α) were transfected with pcDNA3/FLAG (EV) or pcDNA3/FLAG-PHD2 (FLAG-PHD2). After 24h, whole cell extracts (WCEs) were immunoprecipitated with anti-FLAG M2 beads and immunocomplexes were analyzed by Western blot (WB) for the indicated proteins. (D) In vitro translated pcDNA3/FLAG-PHD2 (FLAG-PHD2) or pcDNA3/FLAG (EV) were immunoprecipitated with anti-FLAG M2 beads after incubation with in vitro translated B55α, B55β, B55γ or B55δ and immunocomplexes were detected by WB analysis. (E) WB analysis and quantification of HEK293T cells transiently transfected with HIF1α alone (EV) or in combination with plasmids carrying B55α and/or PHD2 (WT and S125A). (F) HEK293T cells were transfected with a luciferase fused to the oxygen-dependent degradation domain (ODDD-Luc) and either with PHD1, PHD2 or PHD3. After 8h the PP2A inhibitor LB100 (LB; 1μm) was added where indicated for an overnight. Cells were lysed and read at the luminometer. *P<0.05 versus Mock, #P<0.05 versus PHD2; N=3. Graph show mean ± SEM.

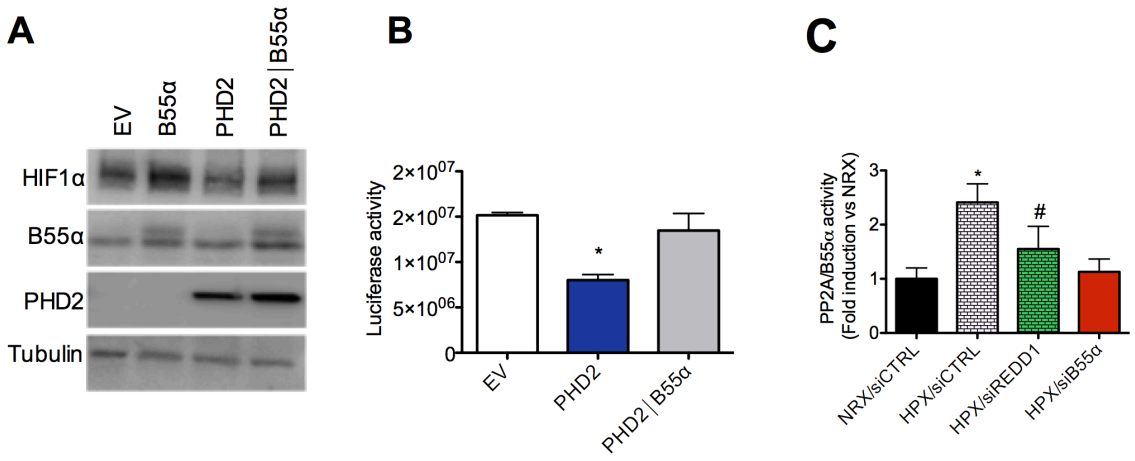

Figure S2, related to Figure 2 and 3. B55α negatively regulates PHD2 function resulting in increased HIF1α protein levels and activity.

(A) WB analysis from HT29 cells transiently transfected with pcDNA3/FLAG (EV), pcDNA3/HA-B55α, pcDNA3/FLAG-PHD2 or both and exposed to hypoxia for 16h.

(B) HEK293T cells stably overexpressing CMV-Luc-ODDD were transiently transfected with pcDNA3/FLAG (EV), pcDNA3/FLAG-PHD2 or pcDNA3/HA-B55α alone and in combination. After 8h the cells were exposed to hypoxia. After 24h cells were lysed and luciferase activity was measured and normalized for protein concentration.

(C) Measurement of the enzymatic activity of PP2A/B55α from WCE of HEK293T cells incubated in normoxia and hypoxia for 16h, as such or after silencing of REDD1. Silencing of B55α (siB55α) was used as negative control. *P<0.05 versus all the other conditions in B and C; # P<0.05 versus HPX16h in C. The graph shows mean ± SEM.

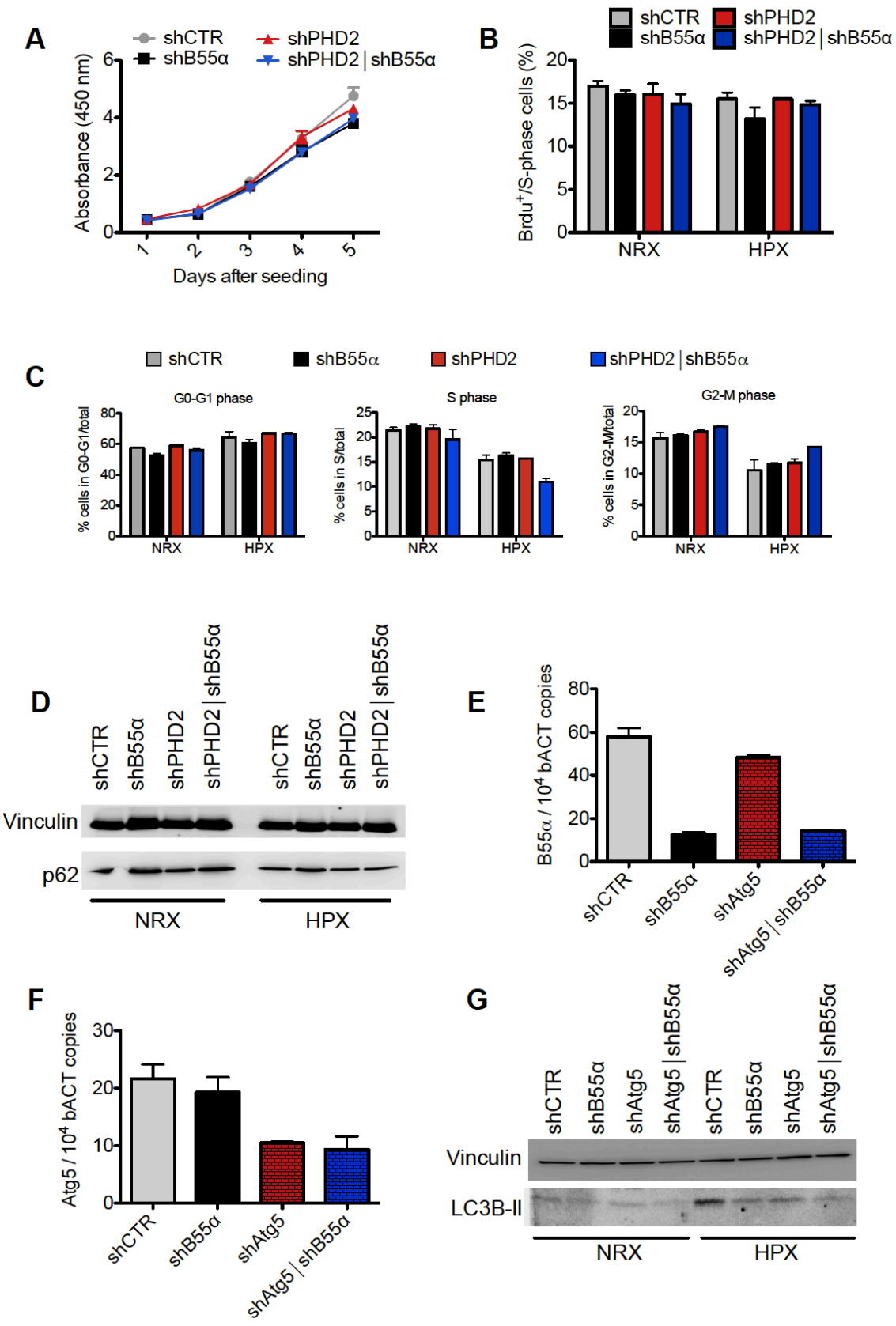
A
shCTR
shB55α
shPHD2
shPHD2 | shB55α
Absorbance (450 nm)
Days after seeding
B
Brdu+/S-phase cells (%)
NRX
HPX
C
G0-G1 phase
S phase
G2-M phase
% cells in G0-G1/total
% cells in S/total
% cells in G2-M/total
D
Vinculin
p62
E
B55α / 10^4 bACT copies
shAtg5
shAtg5 | shB55α
F
Atg5 / 10^4 bACT copies
G
LC3B-II

Figure S3, related to Figure 4. The B55α/PHD2 axis does not modify cell proliferation, but it promotes autophagy in response to hypoxia.

(A) Proliferation curve of DLD1 cells stably silenced for control (shCTR), B55α (shB55α), PHD2 (shPHD2), or both (shPHD2 | shB55α).

(B) BrdU and propidium iodide double staining was performed on DLD1 cells stably silenced for control (shCTR), B55α (shB55α), PHD2 (shPHD2), or both (shPHD2 | shB55α) following 24h in either normoxia (NRX; 21% O_2) or hypoxia (HPX; 0.2% O_2). After 1h incubation with Brdu, cells were fixed and analysed by FACS.

(C and D) DLD1 cells stably silenced for control (shCTR), B55α (shB55α), PHD2 (shPHD2), or both (shPHD2 | shB55α) were exposed to normoxia (NRX; 21% O_2) or hypoxia (HPX; 1% O_2) for 24h. Then cells were stained with propidium iodide and analysed by FACS (C). Same cells as in C were exposed to either normoxia or hypoxia for 48h. Then, WCE were analysed by WB (D).

(E and F) qRT-PCR for B55α (E) and Atg5 (F) in DLD1 cells stably silenced for control (shCTR), B55α (shB55α), Atg5 (shAtg5) or both (shAtg5 | shB55α).

(G) DLD1 stably silenced for control (shCTR), B55α (shB55α), Atg5 (shAtg5) or both (shAtg5 | shB55α) were exposed to normoxia (NRX; 21% O_2) or hypoxia (HPX; 1% O_2) for 48h and WCEs were analysed by WB. All graphs show mean ± SEM.

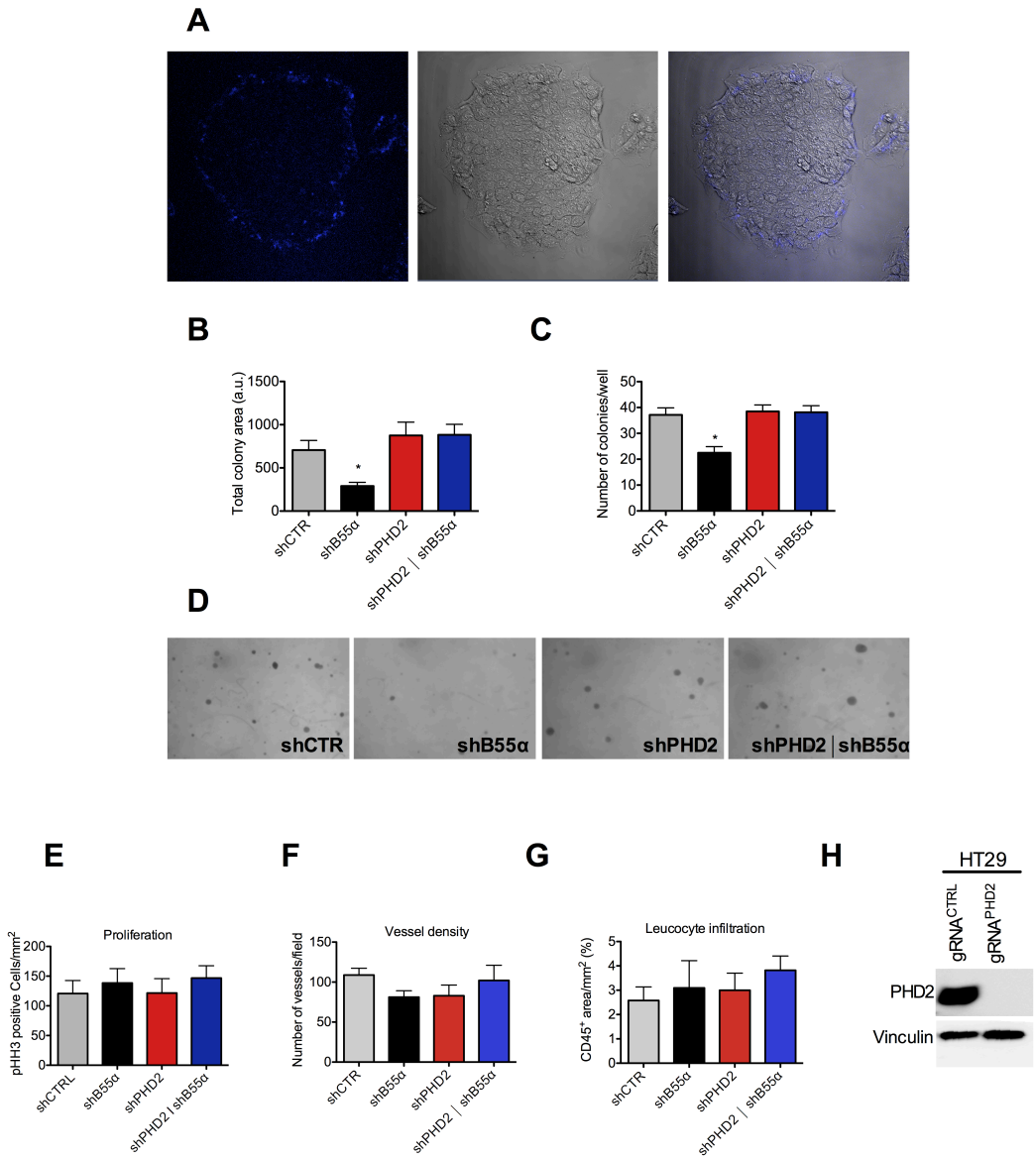

Figure S4, related to Figure 5. PP2A/B55α promotes colorectal cancer growth in a PHD2-dependent manner.

(A) Confocal images of a DLD1-derived foci after 4h incubation with the oxygen-specific probe $NaNO_2$, which labels in blue the oxygenated margin of the colony.

(B-D) Representative pictures and quantification of a soft agar assay with DLD1 cells stably silenced for control (shCTR), B55α (shB55α), PHD2 (shPHD2) or both (shPHD2 | shB55α).

(E) Morphometric quantification of DLD1 tumor sections stained for phosphoHistoneH3, showing proliferation.

(F and G) Morphometric quantification of HT29 tumour sections stained for CD31 showing vessel density (F) and for CD45 showing leucocyte infiltration (G).

(H) WB analysis for PHD2 in HT29 cells transduced with a CRISPR/Cas9 lentiviral construct harbouring a gRNA targeting PHD2 ($gRNA^{PHD2}$) or a non-targeting control ($gRNA^{CTRL}$). *P<0.05 versus all the other conditions. All graphs show mean ± SEM.

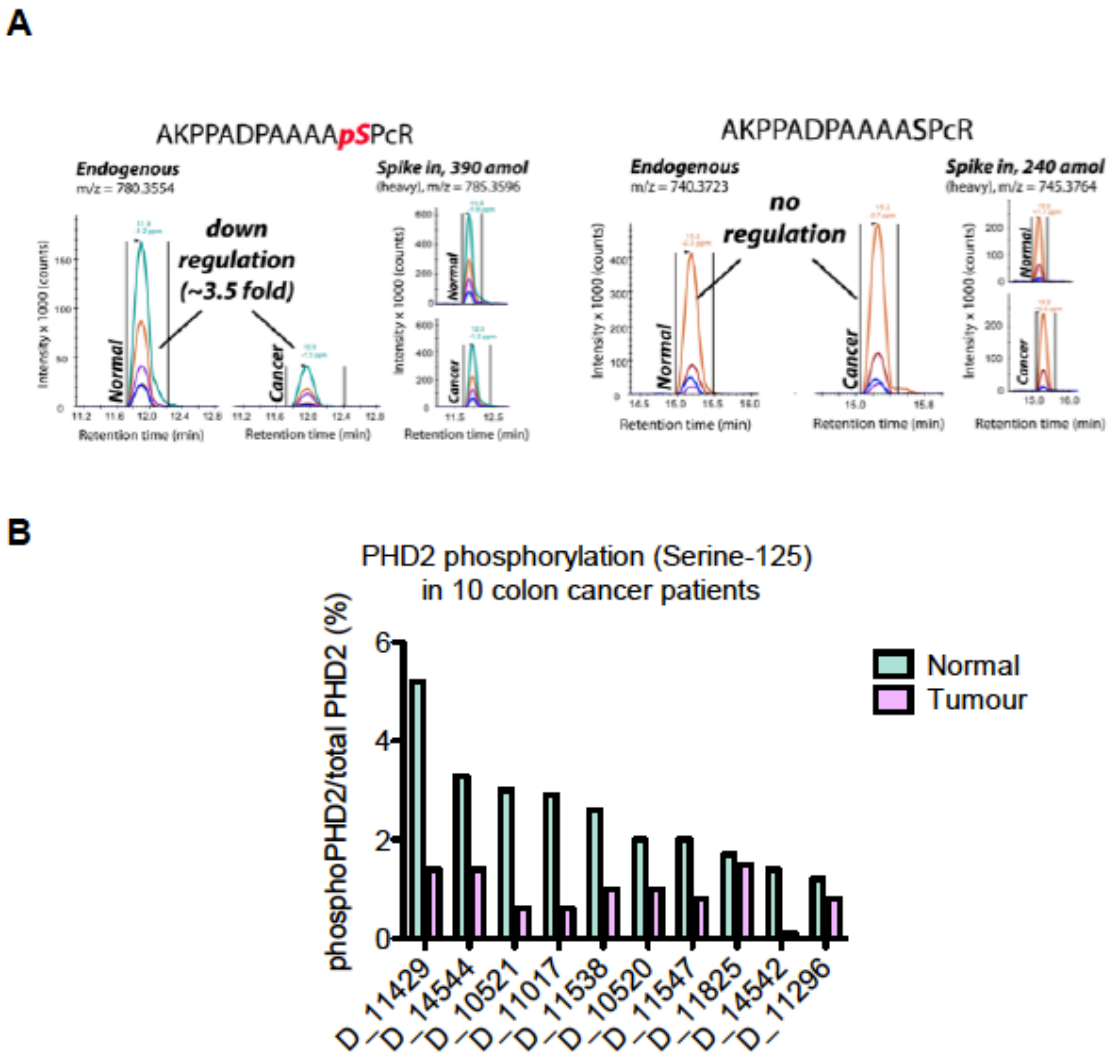

Figure S5, related to Figure 6. In human CRC, phosphorylation of PHD2 in Serine125 is abrogated in tumour samples compared to the healthy tissues.

(A) Targeted PRM to determine PHD2 S-125 phosphorylation stoichiometry in colon cancer and healthy tissue of 10 different patients. For quantification we spiked known amounts of stable-isotopic labelled (SIL) reference peptides to trypsin-digested protein. For quantification of phosphorylated PHD2, we spiked 390 amol of a SIL-peptide in 16 µg of a tryptic digest followed by phosphopeptide enrichment. For the unphosphorylated peptide we used 240 amol of the SIL-peptide in 1.2 µg of tryptic digest. PRM was performed using the 4 or 5 best transitions of each peptide.

(B) Phosphorylation stoichiometry of S-125 PHD2 reveals an average phosphorylation level of 2.5 % in healthy tissue and 0.9 % in cancerous tissue. The phosphorylation stoichiometry is given as percentage of phospho-PHD2 over total PHD2.

Fig 1C								
HIF1α /Vinculin	EV 2.36 ± 0.03	PHD2 0.52 ± 0.04	S12A 0.70 ± 0.05	S14A 0.69 ± 0.06	S125A 1.39 ± 0.061			
Fig 1D								
HIF1α/ Vinculin	EV 0.45 ± 0.05	WT 0.09 ± 0.02	S125A 0.26 ± 0.01	S125D 0.05 ± 0.05				
Fig 1E								
HIF1α/ Tubulin	EV 1.6 ± 0.04	WT 1.05± 0.03	S125A 1.5± 0.01	S125D 0.9± 0.02				
Fig 1F	MG132				HPX			
HIF1α/ Vinculin	EV 2.0±0.05	WT 1.2±0.06	S125A 1.9±0.05	S125D 1.1±0.06	EV 0.36±0.01	WT 0.21±0.04	S125A 0.29±0.01	S125D 0.19±0.04
Fig 1J								
p-PHD2/ total PHD2	Mock 1.35 ± 0.01	Rapamycin 0.61 ± 0.08	Torin2 0.40 ± 0.05	PD169316 1.38 ± 0.06	PD98059 0.95 ± 0.01			

Table S1, related to Figure 1.
Densitometric analysis performed on Western blots run from 3 independent experiments, represented in the indicated panel in Figure 1. All values show mean ± SEM.

			MS human PHD2		MS murine PHD2	
Accession	**Gene name**	**Protein name**	**Log2(L/H)**	**Peptides with valid L/H ratios**	**Log2(L/H)**	**Peptides with valid L/H ratios**
Q91YE3	Egln1	EGL nine homolog 1 (C. elegans)			0,00	26
P52480	PKM2	pyruvate kinase, muscle	1,21	30	1,30	22
Q9GZT9	EGLN1	egl nine homolog 1 (C. elegans)	0,00	15		
Q8BTM8	FLNA	filamin A, alpha			1,18	18
O35465	FKBP8	FK506 binding protein 8, 38kDa			0,01	2
Q6P1F6	**PPP2R2A**	**protein phosphatase 2, regulatory subunit B, alpha (B55α)**	**1,12**	**4**	**1,10**	**3**

Table S2, related to Figure 2. AP-MS data on PHD2 and its interactors.
A SILAC-based strategy was used to identify PHD2 interactors upon PHD2 affinity-based isolation. Log2 (L/H) ratio values are shown, together with the number of identified peptides for which L/H ratio values could be determined. Given the experimental setup, the ratio value for PHD2 was set to zero, and the ratio values for the indicated proteins were corrected. The table shows that known PHD2 interactors and B55α have similar ratio values, hinting to the fact that B55α is a PHD2 interactor.

Fig 2F				
HIF1α/ Vinculin	siCTR/ HIF1α 0.48 ± 0.06	siB55α/ HIF1α 0.13 ± 0.01	siCTR/ HIF1α–PP 0.78 ± 0.03	siB55α/ HIF1α–PP 0.91 ± 0.01
Fig 2G				
p-PHD2/ total PHD2	EV 0.00	PHD2 3.40 ± 0.02	PHD2/B55α 0.92 ± 0.04	S125A 0.00	S125A/B55α 0.00
Fig 2J				
p-PHD2/ total PHD2	EV 0.81 ± 0.03	B55α 0.18 ± 0.001		
Fig 2L				
PHD2/ Vinculin	siCTR 1.10	siCTR 1.24	siCTR 0.92	siB55α 0.78	siB55α 0.96	siB55α 1.05	siP70S6K 1.1	siP70S6K 0.97	siP70S6K 0.93

Table S3, related to Figure 2.
Densitometric analysis performed on Western blots run from 2 or 3 independent experiments, represented in the indicated panel in Figure 2. All values show mean ± SEM.

Fig 3A	HPX			
HIF1α/Tubulin	siCTR 0.89 ± 0.05	siB55α 0.39 ± 0.03	siPHD2 1.30 ± 0.01	siB55α/siPHD2 1.26 ± 0.03
Fig 3B	HPX			
HIF1α/Tubulin	siCTR 1.06 ± 0.02	siB55α 0.481 ± 0.02	siPHD2 1.76 ± 0.01	siB55α/siPHD2 1.93 ± 0.05
Fig 3G	HPX			
HIF1α/Vinculin	siCTR 1.21 ± 0.05	siB55α 0.91 ± 0.01	siREDD1 0.63 ± 0.02	siB55α/siREDD1 0.41 ± 0.05
Fig 3I				
HIF1α/Vinculin	siCTR 1.3 ± 0.02	siB55α 0.7 ± 0.02	siP70S6K 1.9 ± 0.05	siB55α/siP70S6K 2 ± 0.01

Table S4, related to Figure 3.
Densitometric analysis performed on Western blots run from 3 independent experiments, represented in the indicated panel in Figure 3. All values show mean ± SEM.

Fig 4B	NRX				HPX			
CleavPARP/Vinculin	shCTR 0.01±0.02	shB55α 0.15±0.07	shPHD2 0.05±0.04	shPHD2/shB55α 0.12±0.03	shCTR 0.21±0.05	shB55α 0.89±0.01	shPHD2 0.04±0.06	shPHD2/ shB55α 0.23±0.04
Fig 4E	NRX				HPX			
LC3BII / Vinculin	shCTR 0.46±0.01	shB55a 0.4± 0.007	shPHD2 0.4±0.003	shPHD2/ shB55a 0.35±0.03	shCTR 2.3± 0.01	shB55α 1.4± 0.001	shPHD2 2.04±0.05	shPHD2/ shB55α 1.85±0.009
Fig 4G								
HIF1α/ Vinculin	shCTR 1.21±0.04		shB55α 0.78±0.001		HIF1α 2.42±0.01		HIF1α/shB55α 2.9±0.05	
Fig 4I								
LC3BII / Vinculin	shCTR 0.55±0.05		shB55α 0.3±0.006		HIF1α 0.57±0.05		HIF1α/shB55α 0.52±0.032	

Table S5, related to Figure 4
Densitometric analysis performed on Western blots run from 3 independent experiments, represented in the indicated panel in Figure 4. All values show mean ± SEM

Supplemental Experimental Procedures

Plasmids, siRNA and lentiviral vectors. In the overexpression experiments the following plasmids were used: pcDNA3-PHD2-FLAG, pcDNA3 empty vector, pLA-B55α-FLAG, pcDNA3-B55α-HA, pcDNA3-PHD2(S12A), pcDNA3-PHD2(S14A), pcDNA3-PHD2(S125A), pcDNA3-PHD2(S125D), pcDNA3-HIF1α, pDONR223 B55β, pDONR223 B55γ, pDONR223 B55δ. Commercially available siRNAs were purchased from Invitrogen and their sequences or assay IDs are listed below: For B55α: PPP2R2AHSS108371, PPP2R2AHSS108372, PPP2R2AHSS108372 (used alone or in combination); For PHD2: EGLN1HSS123076, EGLN1HSS182577 (used in combination); For scramble: Stealth RNAi™ siRNA Negative Control Lo GC, 12935-200. To generate stable knockdown cell lines, mir-155 miRNA/microRNA lentiviral vectors (shPHD2 and respective scramble (SIMA)) carrying the following shRNA were used: for PHD2: TGCTGTCAACATGACGTACATAACCCGTTTTGGCCACTGACTGACGGGTTATGCGT-CATGTTGA; for the SIMA: TGCTGCATGAATATCTCTGTCTCCTTGTTTTGGCCACTGACTGACAAGGAGACAGATATTCATG Alternatively, PLKO lentiviral vectors (from SIGMA Aldrich) carrying a shB55α, shAtg5 or a scramble sequence as control, were used: for B55α: CCGGAGAAACACAAAGCGAGACATACTCGAGTATGTCTCGCTTTGTGTTTCTTTTTT; for Atg5: CCGGGATTCATGGAATTGAGCCAATCTCGAGATTGGCTCAATTCCATGAATCTTTTTTG; for the scramble: CCGGCAACAAGATGAAGAGCACCAACTCGAGTTGGTGCTCTTCATCTTGTTGTTTTT. For the overexpression of HIF1 and control the following lentiviral vectors were used: pLenti/UbC/V5-Dest-hHIF1a-deltaProline-V5 pLenti/UbC/LacZ control. Selection with Blasticidin (10 μg/ml) or puromycin (4 μg/ml) allowed the generation of a homogenous population of silenced or overexpressed (and scramble control) cells.

Western Blot analysis. Protein extraction was performed using RIPA lysis buffer (50 mM Tris HCl pH 8, 150 mM NaCl, 1% Triton X-100, 0.5% sodium deoxycholate, 0.1% SDS) supplemented with Complete Protease Inhibitor Cocktail (Roche) and PhosSTOP phosphatase inhibitor (Roche). Lysates were incubated on ice for 30 minutes before centrifuging 15 minutes at 4°C to remove cellular debris. Supernatants were subsequently collected. Protein concentration of cell extracts was determined by using bicinchoninic acid (BCA) reagent (Pierce) according to the manufacturer's instructions. Protein samples were denaturated by adding loading buffer 6X (β-mercaptoetanolo 0,6 M; SDS 8%; Tris-HCl 0,25 M pH 6,8; glycerol 40%; Bromophenol Blue 0,2%), incubated at 95°C for 5 minutes. After electrophoresis, proteins were transferred onto a nitrocellulose membrane using the iBlot® Dry Blotting System (Invitrogen) according to manufacturer's instructions. The membranes were blocked for non-specific binding in 5% non-fatty dry milk in Tris Buffered Saline-Tween 0.1 % (50 mM Tris HCl ph 7.6, 150 mM NaCl, 0.1% Tween; TBS-T) for 1h at room temperature (RT) and incubated with primary antibody for 2h at RT or overnight (ON) at 4°C. The following antibodies were used: PPP2R2A/B55α (Clone 2G9, Cell Signaling); EGLN1 (human PHD2) (NB-100-137, Novus Biological); Vinculin (Monoclonal anti-Vinculin, V9131, SIGMA Aldrich); Tubulin (HRP-conjugated anti-beta-tubulin, Abcam); HIF1α (human HIF1α, Cayman Chemical); Hydroxy-HIF1α (Clone D43B5, Cell Signaling); FLAG (Monoclonal anti-FLAG, SIGMA Aldrich); PP2A Ca (Clone 46, BD Bioscience); Cleaved PARP (rabbit, Cell Signaling); LC3B (Clone D11, Cell Signaling); SQSTM1 (p62) (Clone 2C11, Abnova), phosphoP70S6K (Thr389) (Cell Signaling); P70S6K (Clone 49D7, Cell Signaling); phospho-S125PHD2 (MABC1612 clone 4, Merck).
After incubation with the indicated primary antibodies, the membranes were washed for 15 minutes in TBS-T and incubated with secondary antibody (1/5000 in 5% non fatty dry milk in TBS-T) for 50 minutes at RT. The following secondary antibodies were used: goat anti-mouse and goat anti-rabbit (Santa Cruz biotechnology). The signal was visualized with Enhanced Chemiluminescent Reagents (ECL; Invitrogen) or SuperSignal West Femto Chemiluminescent Substrate (Thermo Scientific) with a digital imager (ImageQuant LAS 4000, GE Health Care Life Science Technologies).

Immunoprecipitation. Cells were lysed using Extraction Buffer (EB; 1% triton, 20 mM Tris, 10% glycerol, 5 mM EDTA, 150 mM NaCl, pH 7.4). Protein extraction and determination of protein concentration were performed as described. For anti-FLAG immunoprecipitations, 1 or 2 mg of total protein was incubated with anti-FLAG M2 affinity gel (Sigma-Aldrich®) followed by elution with FLAG-peptide, according to manufacturer's instructions. For endogenous co-immunoprecipitations, antibody anti-PHD2 (Novus Biological) was incubated for 2h at 4°C with magnetic Dynabeads Protein G (Life Technology) in PBS Tween 0.05% and afterwards the beads-antibody complexes were incubated 30' at 4°C with BS_3 (Sulfo-DSS, Thermo Scientific), a water soluble cross-linker in Conjugation buffer (pH 7-9) 20 mM Sodium Phosphate, 0.15 M NaCl (pH 7-9). Two mg of protein extracts from DLD1 or HT29 were incubated overnight with beads-Antibody conjugated. Immunoprecipitates were washed 3 times with EB Buffer and 3 times with TBS-Tween 0.1%. For the bead elution, NuPage LDS sample buffer (Novex, without 2-Mercaptoethanol) was added to the immunocomplexes and incubate for 10 min at 99 ºC. Supernatant was collected and denaturated by adding DTT 20mM for 10' at 99°C. Electrophoresis and Western blot were performed as described. For in vitro co-immunoprecipitation, in vitro translated FLAG-PHD2 or HA-B55a were produced by using TNT coupled wheat germ extract system/T7 promoter (Promega) according to manufacturer's instructions. 20 ml of the 50 ml reaction proteins were incubated with each other for 2 hours at 4°C in EB lysis buffer. Therefore, anti-FLAG IP was performed as previously described.

Luciferase assay. HEK293T or DLD1 cells were stably transfected with a plasmid carrying CMV-Luc-ODD (O_2-dependent degradation domain). Medium was changed every two days with culture medium containing 100 mg/ml G418 for 15 days until a homogenous population of ODDD-overexpressing cells was obtained. Subsequently, selected cells were transiently transfected with the indicated plasmids or siRNA. Alternatively DLD1 cells stably silenced for PHD2 or B55A or both, were transiently transfected with a construct encoding CMV-HRE-Luc. Cells were lysed in luciferase lysis buffer (PBS, 0.2% Triton X-100, 0.5% DTT) and luminescence was measured by using a luminometer (Microplate Luminometer LB 96 V), in presence of a luciferase Assay Reagent (CoA 500 mM, Luciferin 500 mM, ATP 1000 mM and luciferase assay buffer (20 mM, ($MgCO_3$) $4Mg(HO)_2.5H_2O$ 1.07 mM, $MgSO_4$ 2.67 mM, EDTA 0.1 mM, DTT 33.3 mM in H_2O). Luciferase activity was normalized for protein content, as determined by BCA.

Liquid Chromatography-Mass Spectrometry (LC-MS) to identify PHD2 phosphorylation sites. To identify PHD2 phosphorylation sites, overexpression of FLAG-tagged PHD2 has been performed in HEK293T cells. Cells were harvested, lysed in extraction buffer and 3 mg of total protein extracts was used for immunoprecipitation using anti-FLAG M2 affinity beads, as previously described. Immunoprecipitated proteins were separated by SDS-PAGE and stained using Coomassie. Gel bands of interest were excised, washed several times with water and acetonitrile, and completely dried in a SpeedVac. Subsequently, an in-gel trypsin digest was performed using sequence-grade modified trypsin, porcine (Promega, Madison, Wi USA) and samples were incubated overnight at 37°C. The supernatants containing the peptides were then isolated, transferred to MS-compatible vials and acidified with trifluoroacetic acid (TFA) (pH < 3). The obtained peptide mixtures were introduced into an LC-MS/MS system; the Ultimate 3000 RSLC nano (Dionex, Amsterdam, The Netherlands) in-line connected to an LTQ Orbitrap Velos (Thermo Fisher Scientific, Bremen, Germany) for analysis. Peptides were first loaded on a trapping column (made in-house, 100 mm internal diameter (I.D.) x 20 mm, 5 mm C18 Reprosil-HD beads, Dr. Maisch, Ammerbuch-Entringen, Germany). After back-flushing from the trapping column, the sample was loaded on a reverse-phase column (made in-house, 75 µm I.D. x 150 mm, 3 µm C18 Reprosil-HD beads, Dr. Maisch). Peptides were loaded with solvent A (0.1% TFA, 2% acetonitrile) and separated with a linear gradient from 98% solvent A' (0.1% formic acid in water) to 55% solvent B' (0.1% TFA, 80% ACN) at a flow rate of 300 nl/min followed by a wash reaching 100% solvent B'. The mass spectrometer was operated in data-dependent mode, automatically switching between MS and MS/MS acquisition for the ten most abundant peaks in a given MS spectrum. In the LTQ-Orbitrap Velos, full scan MS spectra were acquired in the Orbitrap at a target value of 1E6 with a resolution of 60,000. The ten most intense ions were then isolated for fragmentation in the linear ion trap, with a dynamic exclusion of 40 s. Peptides were fragmented after filling the ion trap at a target value of 1E4 ion counts. From the MS/MS data in each LC run, Mascot Generic Files were created using Distiller software (version 2.4.3.3, Matrix Science, www.matrixscience.com/Distiller). While generating these peak lists, grouping of spectra was allowed in Distiller with a maximum intermediate retention time of 30 s and a maximum intermediate scan count of 5

was used where possible. Grouping was done with 0.005 Da precursor tolerance. A peak list was only generated when the MS/MS spectrum contained more than 10 peaks. There was no deisotoping and the relative signal to noise limit was set at 2. These peak lists were then searched with Mascot search engine (MatrixScience) using the Mascot Daemon interface (version 2.3.01, Matrix Science). Spectra were searched against the Swiss-Prot database restricted to *Homo sapiens* (SwissProt 2012_04, 20.324 protein sequences). Variable modifications were set to pyro-glutamate formation of amino-terminal glutamine, acetylation of the protein N-terminus, oxidation of methionine, hydroxylation of proline, propionamidation of cysteine and phosphorylation on serine, threonine and tyrosine. Tolerance on precursor ions was set to ± 10 ppm (with Mascot's C13 option set to 1) and on fragment ions to ± 0.5 Da. The peptide charge was set to 2+, 3+, and the instrument setting was put on ESI-TRAP. Enzyme was set to trypsin, allowing for one missed cleavage, also cleavage was allowed when arginine or lysine is followed by proline. Only peptides that were ranked one and scored above the threshold score, set at 99% confidence, were withheld. All data management was done by ms_lims (PMID: 20058248).

Targeted LC-MS to determine PHD2 S125 phosphorylation levels. Targeted LC-MS to determine PHD2 S125 phosphorylation levels. To determine the levels of phosphorylated and unphosphorylated PHD2 (serine 125) in cell culture and patient samples, we performed bottom-up proteomics and phosphoproteomics. The purified protein fraction of each sample was digested using trypsin followed by spike-in of stable-isotope-labelled (SIL-) reference peptides of known concentrations. The known concentrations of the SIL-peptides enabled an LC-MS-based quantification of the peptides derived from endogenous PHD2 upon digestion.

For targeting the more abundant unphosphorylated peptide in patient samples, non-fractionated tryptic digests were analyzed by LC-MS. For targeting the unphosphorylated peptide in cell culture samples and the phosphorylated peptide in all samples, we introduced an additional purification step by HPLC: Using the corresponding SIL peptides, we determined the retention times (I) of the unphosphorylated peptide in high-pH-reversed phase separation and (II) the retention time of the phosphorylated peptide in electrostatic repulsion-hydrophilic interaction chromatography (ERLIC) (Alpert, 2008; Loroch et al, 2015). Afterwards, samples were separated using the same conditions to collect a fraction at the specific retention times to yield a crude enrichment of the target peptides. Subsequent LC-MS analysis was done in parallel reaction monitoring (PRM) mode.

Experimental details are given in the following sections:

i) Synthesis and amino acid analysis of stable-isotope-labelled (SIL-) reference peptides:

Unphosphorylated and phosphorylated fully tryptic reference peptides (AKPPAD**P**AAAASPC**R)** containing PHD2 S125 were synthesized in-house using a Syro I synthesis unit (MultiSynTech, Witten, Germany) and Fmoc chemistry**.** A heavy-labelled arginine was incorporated at the C-terminus resulting in a mass shift of +10.0083 Da. Peptides were purified by preparative RP-LC coupled via a 1:20 split to an MS-Q (Thermo Fisher, Bremen, Germany) mass spectrometer for targeted fractionation. After lyophilization, peptides were solubilized in 0.1 % TFA and the peptide concentration was determined using amino acid analysis according to Cohen et al. (Cohen & Michaud, 1993). Quantification was conducted against a five-point calibration curve of derivatized amino acids in the range from (5 -25 pmol/µL).

ii) Sample processing: Samples were lysed using 1% SDS containing 1 tablet of PhosSTOP and 1 tablet Complete mini (Roche, Mannheim, Germany) per 10 mL. Samples were lysed by 2 cycles of ultrasonication on ice. Debris was removed by centrifugation at 16,000 g for 20 min at 4°C. Proteins were precipitated by adding 9 volumes of ice-cold ethanol, followed by incubation at -40° C for 1 h. Precipitates were spun down at 20,000 g for 40 minutes at 4° C and pellets were washed using 50 µL of ice-cold acetone. Protein pellets were solubilized in 6 M guanidinium-HCl followed by protein concentration determination using a BCA kit (Pierce by Thermo Scientific, Bremen, Germany). Afterwards, samples were adjusted to equal protein concentrations using 6 M guanidinium-HCl. Prior to proteolytic digestion, samples were diluted 20-fold using 50 mM ammonium bicarbonate, 1.5 mM $CaCl_2$. Trypsin (Sequencing grade, Promega, Mannheim, Germany) was added in a ratio of 1:10 (Dickhut et al, 2014) (trypsin : protein) and samples were incubated for 15 h at 37° C with slight agitation (for cell culture experiments, 100 µg of protein and for patient samples 70 µg were digested). The digestion was stopped by adding FA to a final concentration of 1% and peptides were purified using SPEC-C18 AR cartridges (Agilent, Boeblingen, Germany). Digests were quality controlled using a monolithic column HPLC separation, as described previously (Burkhart et al, 2012).

iii) Purification of the unphosphorylated peptide using HPLC-based high-pH-RP: High-pH-RP was done with an U3000 HPLC (Thermo Fisher, Bremen, Germany) equipped with a Biobasic-C18 column, 0.5 mm x 15 cm, 5 µm (Thermo Scientific). The binary gradient (12.5 µL/min) consisting of solvent A: 10 mM ammonium formate, pH 8 and solvent B: 84% (v/v) in 10 mM NH_4HCO_2, pH 8.0 was as follows: equilibration for 20 min with 3% B, followed by 3% B for 7 min, 3% to 31.5% B (linear) in 21.5 min, and 31.5% to 95% B in 15 min, 95% B for 2.5 min before returning to 3% B. A linear gradient from 3 to 95% B was used to wash the column between each of the runs.

We determined the retention time of the target peptide using 2 pmol of the SIL peptide (minute 17.5). Afterwards 12 µg of each sample including 600 amol of the SIL-peptide were injected in 15 µL of buffer A and a 2.5-minute fraction was collected at the specific retention time (± 1.25 min). All fractions were dried in a vacuum centrifuge and re-dissolved in 0.1% TFA for LC-MS analysis.

iv) Purification of the phosphorylated peptide using ERLIC: ERLIC was done with an Ultimate HPLC (Thermo Fisher, Bremen, Germany) equipped with a PolyWAX (weak anion exchange) column (2.1 mm × 200 mm, 5 µm, 300 Å, Poly LC, Columbia). The binary gradient (200 µL/min) consisting of solvent A': 20 mM sodium methylphosphonic acid, 70% acetonitrile (ACN), pH 2 and solvent B': 200 mM triethylammonium phosphate, 60% ACN, pH 2 was as follows: equilibration for 25 min with 100% A', followed by 100% A' for 10 min, 0% to 100% B' (linear) in 5 min, 100% B' for 10 min, followed by 100% A' for re-equilibration. A linear gradient from 0 to 100 % B was used to wash the column between each of the runs.

We determined the retention time of the target phosphopeptide using 400 pmol of the SIL-phosphopeptide. Afterwards, we spiked 2 fmol of the SIL-phosphopeptide into 30 µg (cell culture experiments) or 790 amol in 32 µg (patient tissue) of the tryptic digest. Samples were injected to ERLIC in 20 µL of buffer A' and a 4-minute fraction was collected at the specific retention time (± 2 min). Fractions were dried under vacuum, reconstituted in 0.1% trifluoroacetic acid (TFA) and desalted using Hypersep C18-RP 10-200 µL cartridges (Thermo Fisher). Peptides were eluted from the cartridge with 30% ACN. Samples were dried under vacuum and reconstituted in 0.1 % TFA.

v) Targeted LC-MS analysis: Targeted LC-MS analysis was done in parallel reaction monitoring (PRM) mode to absolutely quantify endogenous levels of the phosphorylated and unphosphorylated peptides in each sample using the known concentrations of the SIL peptides. PRM was performed using a Q-Exactive HF mass spectrometer online coupled to a U3000 RSLC nanoHPLC equipped with an Acclaim PepMap trap-column (100 µm x 2 cm, 5 µm particles, 100 Å pores) and an Acclaim PepMap main column (75 µm x 50 cm, 3 µm particles, 100 Å pores). Peptides were injected onto the trap column in 0.1% TFA using a flow rate of 10 µL/min. After 5 min the trap column was switched in-line and peptides were separated using a 1 h gradient ranging from 2.5 to 40 % ACN in 0.1% FA at a flow rate of 250 nL/min. For quantification of the unphosphorylated peptide in patients samples, 240 amol of the unphosphorylated SIL-peptide were spiked in 1,2 µg of tryptic digest prior to LC-MS. For quantification of the unphosphorylated peptide in cell culture samples, 50% of each high-pH-RP fraction was analyzed (corresponding to 6 µg digest + 300 amol of SIL peptide). PRM was conducted using the m/z of the +2 and +3 charged ions of both the endogenous (m/z: 740.3723 and 493.9173) and the SIL-peptide (m/z: 745.3764 and 497.2534).

Fragmentation was done using a 0.4 m/z isolation window and a normalized collision energy of 27. Fragment ion spectra were acquired at a resolution of 30,000; automatic gain control (AGC) was set to 2 x 10^5 with a maximum injection time of 500 ms.

For quantification of the phosphopeptide 50% of each ERLIC-sample were used (corresponding to 15 µg digest + 1 fmol SIL-phosphopeptide) and PRM was conducted using the m/z of the +2 and +3 charged ions of both the endogenous (m/z: 780.3554 and 520.5727) and the SIL-phosphopeptide (m/z: 785.3596 and 523.9088) and the same parameters as for the unphosphorylated peptide but with an AGC target value of 10^5.

vi) Data analysis: Raw-files were imported into Skyline v3.1 (MacLean et al, 2010) and the 3 to 5 best transitions of each peptide were manually selected and used for quantification. Obtained peptide ratios were exported to Excel and the amount of each peptide per µg of tryptic digest was calculated (in amol*µg digest^{-1}). Phosphorylation stoichiometry was determined using the following equation:

$$\%\,phosphorylation = \frac{amol_{phosphorylated}}{\mu g_{digest}} \cdot \frac{\mu g_{digest}}{\mathrm{amol}_{\mathrm{phosphorylated}} + \mathrm{amol}_{\mathrm{unphosphorylated}}} \cdot 100\%$$

In Vivo Labeling with [^{32}P]Orthophosphate and Immunoprecipitation. DLD1 cells were cultured in a humidified incubator at 37° C and 5% CO_2. The next day, the cells were washed with phosphate-free DMEM (Gibco) and incubated with the same medium containing 1 mCi of [^{32}P]orthophosphoric acid (NEN)/ml (PerkinElmer, Groningen, Netherlands) under hypoxic conditions (37°C, 5% CO_2 and 1% O_2). At indicated time points, cells were washed twice with ice-cold PBS and scraped in lysis buffer (50 mM Tris/HCL, pH 7.5, 150 nM NaCl, 1% Titon X-100, 2 mM EDTA, 2 mM EGTD, 1 mM PMSF and proteasome inhibitor cocktail tablet (Roche)). To recover endogenous PHD2, equal amounts of total protein (500 µg) were incubated with 4 µg of PHD2 antibody for 2 h at 4˚C before Sepharose beads (30 µl per reaction) were added overnight at 4˚C. Thereafter, the beads were washed five times with lysis buffer, recovered and pellets were dissolved in 2 X Laemmli buffer, boiled at 95˚C for 7 min and separated by 10% SDS PAGE. Afterwards, the gel was blotted onto a nitrocellulose membrane and the membrane was exposed to a KODAK phosphor imaging screen overnight. Autoradiography was detected with MolecularImager FX using the Quantity One software (all BioRad, Helsinki, Finland). Thereafter, the membrane was probed with an antibody against PHD2.

Propidium Iodide Staining. Supernatants derived from DLD1 and HT29 cells cultured in normoxia or hypoxia was collected in order to keep dead cells. Adherent cells were subsequently trypsinized, added to the supernatant previously collected and centrifuged at 300g for 5 minutes. After one wash with PBS, cells were fixed with 1 ml of 70% ethanol. Cells were incubated 2h or overnight at 4°C, prior to another centrifugation at 300g for 5 minutes. Supernatant was removed and the pellet was resuspended in 200 µl of PBS, containing 500 µg of RNase (10 mg/ml). 200 ml of Propidium Iodide (0,1mg/ml) was added to a final volume of 400 µl. Samples were incubated for 1-2 h at 37°C and subsequently analyzed by Fluorescence-Activated Cell Sorting by using FACS Canto II (BD Bioscience).

Immunocytochemistry. 2x10^5 DLD1 cells transfected with FLAG-PHD2WT, S125A and S125D were seeded on top of sterilized, gelatin treated coverslips in 6-well dishes. Cells were rinsed three times with PBS and fixed in methanol for 20 minutes on ice. Cells were washed two times with PBS and permeabilized and blocked for 1 hour in PBS 0.1% Triton 5% BSA at room temperature (RT). Coverslips were incubated with primary antibody (FLAG, 1:100, SIGMA Aldrich) in blocking solution (PBS, 5% BSA) for 2 hours. Cells were washed with PBS three times for 10 minutes, rinsed with blocking solution, and incubated for 1 hour with 1/500 donkey anti-rabbit-Alexa 568 in blocking solution. Cells were washed once with blocking solution and three times for 10 minutes with PBS before mounting coverslips with prolong gold with DAPI (Life Technologies).

Proliferation assays. For cell proliferation, 10 µM of BrdU was added to the cells previously incubated in normoxia or hypoxia. After 1 hour, cell proliferation was quantified on single cell suspensions with the FITC BrdU Flow Kit (BD Bioscience) according to manufacturer's protocol. Alternatively, cells were seeded in triplicate in 5 96-well plate. Proliferating cells were detected every 24 hours for 5 days by using Cell Proliferation Reagent WST1 (Roche Diagnostics), according to manufacturer's protocol.

Immunocytochemistry. 2x10^5 DLD1 cells were seeded on top of sterilized, gelatin treated coverslips in 6-well dishes and subsequently incubated in normoxia or hypoxia (0.2% O_2) for 48 hours. Cells were rinsed three times with PBS and fixed in methanol for 20 minutes on ice. Cells were washed two times with PBS and permeabilized and blocked for 1 hour in PBS 0.1% Triton 5% BSA at room temperature (RT). Immunostaining was performed on coverslips by using ApopTag Fluorescein Direct In Situ Apoptosis Detection Kit (Millipore) according to manufacturer's instructions. Prolong gold with DAPI (Life Technologies) was used to detect cell nuclei.

Quantitative Real Time Polymerase Chain Reaction (qRT-PCR). To assess gene expression, RNA from DLD1 or HT29 seeded in triplicate in 12-well plates was extracted with a RNeasy Mini kit (Qiagen) according to manufacturer's instructions. Reverse transcription to cDNA was performed by using Quantitect Reverse Transcription Kit (Qiagen) according to manufacturer's protocol. cDNA, primer/probe mix and TaqMan Fast Universal PCR Master Mix were prepared in a volume of 10 ml according to manufacturer's instructions (Applied Biosystems). qRT-PCR was performed in an Applied Biosystems 7500 Fast Real-Time PCR system. Pre-made assays were purchased and their assay IDs are listed below:
PPP2R2A (B55a): Hs.PT.58.25465949 from IDT

bActin: Hs.PT.39a.22214847 from IDT
BNIP3: Hs.PT.56a.404067 from IDT
BNIP3L: Hs.PT.56a.1103799 from IDT
EGLN1 (PHD2): Hs00254393_m1 from Applied Biosystem
bActin: Hs99999903_m1 from Applied Biosystem.

Hypoxia assessment. Tumor hypoxia was detected by injection of 60 mg/kg pimonidazole hydrochloride into tumor-bearing mice 1 hour before tumor harvesting. To detect the formation of pimonidazole adducts, tumor cryosections were immunostained with Hypoxyprobe-1-Mab1 (Hypoxyprobe kit, Chemicon) following the manufacturer's instructions.

Histology and immunostainings. To obtain serial 7-μm-thick sections, tissue samples were immediately frozen in OCT compound or fixed in 2% PFA overnight at 4°C, dehydrated and embedded in paraffin. Paraffin slides were first rehydrated to further proceed with antigen retrieval in citrate solution (DAKO). Cryo-sections were thawed in water and fixed in 100% methanol. If necessary, 0.3% H_2O_2 was added to methanol to block endogenous peroxidases. The sections were blocked with the appropriate serum (DAKO) and incubated overnight with the antibody rabbit anti-LC3B (Cell Signaling; clone D11) 1:200 and Hypoxyprobe-1-Mab1. Appropriate secondary antibodies were used: Alexa488-or Alexa568-conjugated secondary antibodies (Molecular Probes) 1:200. When necessary, Tyramide Signaling Amplification (Perkin Elmer, Life Sciences) was performed according to the manufacturer's instructions. Whenever sections were stained in fluorescence, ProLong Gold mounting medium with DAPI (Invitrogen) was used. Otherwise, 3,3'-diaminobenzidine was used as detection method followed by Harris' haematoxilin counterstaining, dehydration and mounting with DPX. Apoptotic cells were detected by the TUNEL method, using the ApopTag peroxidase in situ apoptosis detection kit (Millipore) according to the manufacturer's instructions. Microscopic analysis was done with an Olympus BX41 microscope and CellSense imaging software. The analysis was performed by acquiring 4-6 fields per sections on 5 independent sections from the same biological tissue sample. The values in the graphs represent the average of the means of, at least, 5 samples and the standard error indicates the variability among the different samples.

Dephosphorylation assay. FLAG-PHD2 isolated from HEK293T cells was incubated alone or with immune-purified FLAG-B55α in dephosphorylation buffer (100 mM Tris-Cl, pH 7.4, 100 mM KCl, 20 mM $MgCl_2$, 30 mM EGTA) for 30' at 30°C.

Generation of CRISPR/Cas9 constructs. The lentiCRISPR v2 was a gift from Feng Zhang (Addgene plasmid # 52961). The gRNA targeting PHD2 exon 1 (CGGACAGCAGATCGGCGACG) was generated using Rule Set 2 (Doench et al, 2016). PHD2 targeting gRNA and non-targeting control gRNA (GAACAGTCGCGTTTGCGACT) were then cloned in lentiCRISPR v2 as described previously (Sanjana et al, 2014). A silent mutation was introduced within the PHD2 coding sequences ($PHD2^{wt}$, $PHD2^{S125A}$ and $PHD2^{S125D}$) in order to remove the protospacer adjacent motif (PAM) sequence that is absolutely necessary for CRISPR/Cas9 target binding. The cDNAs were then PCR amplified and cloned into a lentiviral vector after restriction with AgeI/SpeI.

Supplemental References

Alpert AJ (2008) Electrostatic repulsion hydrophilic interaction chromatography for isocratic separation of charged solutes and selective isolation of phosphopeptides. *Anal Chem* **80:** 62-76

Burkhart JM, Schumbrutzki C, Wortelkamp S, Sickmann A, Zahedi RP (2012) Systematic and quantitative comparison of digest efficiency and specificity reveals the impact of trypsin quality on MS-based proteomics. *Journal of proteomics* **75:** 1454-1462

Cohen SA, Michaud DP (1993) Synthesis of a fluorescent derivatizing reagent, 6-aminoquinolyl-N-hydroxysuccinimidyl carbamate, and its application for the analysis of hydrolysate amino acids via high-performance liquid chromatography. *Analytical biochemistry* **211:** 279-287

Dickhut C, Feldmann I, Lambert J, Zahedi RP (2014) Impact of digestion conditions on phosphoproteomics. *Journal of proteome research* **13:** 2761-2770

Doench JG, Fusi N, Sullender M, Hegde M, Vaimberg EW, Donovan KF, Smith I, Tothova Z, Wilen C, Orchard R, Virgin HW, Listgarten J, Root DE (2016) Optimized sgRNA design to maximize activity and minimize off-target effects of CRISPR-Cas9. *Nat Biotechnol* **34:** 184-191

Loroch S, Zahedi RP, Sickmann A (2015) Highly sensitive phosphoproteomics by tailoring solid-phase extraction to electrostatic repulsion-hydrophilic interaction chromatography. *Anal Chem* **87:** 1596-1604

MacLean B, Tomazela DM, Shulman N, Chambers M, Finney GL, Frewen B, Kern R, Tabb DL, Liebler DC, MacCoss MJ (2010) Skyline: an open source document editor for creating and analyzing targeted proteomics experiments. *Bioinformatics (Oxford, England)* **26:** 966-968

Sanjana NE, Shalem O, Zhang F (2014) Improved vectors and genome-wide libraries for CRISPR screening. *Nat Methods* **11:** 783-784